Enterotoxigenic *Escherichia coli* heat-labile toxin drives enteropathic changes in small intestinal epithelia

Alaullah Sheikh[1], Brunda Tumala[1], Tim J. Vickers[1], John C. Martin[2], Bruce A. Rosa[1,2], Subrata Sabui[5,6], Supratim Basu[1], Rita D. Simoes[1], Makedonka Mitreva[1,2], Chad Storer[2,3], Erik Tyksen[2,3], Richard D. Head[2,3], Wandy Beatty[4], Hamid M. Said[5,6], and James M. Fleckenstein[1,7].

Division of Infectious Diseases[1], Department of Medicine, Washington University School of Medicine, St. Louis, MO 63110, USA.

The McDonnell Genome Institute[2], Washington University School of Medicine, St. Louis, MO 63110, USA.

Department of Genetics[3], Washington University School of Medicine, St. Louis, MO 63110, USA.

Department of Molecular Microbiology[4], Washington University School of Medicine, Saint Louis, Missouri, USA 63110.

Departments of Medicine and Physiology/Biophysics, School of Medicine, University of California-Irvine, Irvine, CA[5]; 92697.

Department of Research, VA Medical Center, Long Beach, CA[6]; 90822

Infectious Diseases, Medicine Service, Veterans Affairs Saint Louis Health Care System, Saint Louis Missouri, USA 63106[7].

corresponding author
James M. Fleckenstein
Division of Infectious Diseases
Department of Medicine
Washington University School of Medicine
Campus Box 8051
660 South Euclid Avenue
Saint Louis Missouri, USA 63110
p 314-362-9218
jfleckenstein@wustl.edu

abstract

Enterotoxigenic *E. coli* (ETEC), produce heat-labile (LT) and/or heat-stable (ST) enterotoxins, and are a common cause of diarrhea in children of resource-poor regions. ETEC have also been linked repeatedly to poorly understood sequelae including enteropathy, malnutrition, and growth impairment. While the cellular actions of ETEC enterotoxins leading to diarrhea are well-established, their potential contribution to subsequent pathology is unclear. LT stimulates cellular cAMP production to activate protein kinase A (PKA) which phosphorylates cellular ion channels that drive export of salt and water into the intestinal lumen resulting in diarrhea. However, as PKA exhibits broad kinase activity and its activated catalytic subunits modulate transcription of many genes, we interrogated the transcriptional profiles of LT-treated small intestinal epithelia. These studies demonstrated toxin-induced changes in hundreds of genes including those required for biogenesis and function of the brush border, the major site absorption of nutrients, and suppression of a key transcription factor, HNF4, critical to differentiation of intestinal epithelia. Accordingly, LT treatment of intestinal epithelial cells significantly disrupted the absorptive microvillus architecture and altered transport of essential nutrients. In addition, challenge of neonatal mice with LT-producing ETEC recapitulated the architectural derangement of the brush border while maternal vaccination with LT prevented brush border disruption in ETEC-challenged neonatal mice. These findings highlight impacts of ETEC enterotoxins beyond acute diarrheal illness and may inform approaches to mitigate and prevent major sequelae including malnutrition that impact millions of young children.

54

55 ## Introduction

56 Infectious diarrhea remains a leading cause of death and morbidity among young children in low-
57 middle income countries where access to clean water and sanitation remain in short supply[1].
58 Enterotoxigenic *E. coli* (ETEC), initially discovered as a cause of severe, cholera-like illness[2], are one
59 of the most common pathogens associated with moderate-severe diarrhea among children under
60 the age of five years[3,4], and are perennially the most common cause of diarrhea in travelers[5] to
61 endemic regions where these organisms are thought to account for hundreds of millions of cases of
62 diarrheal illness each year[6].

63 Importantly, ETEC infections have been linked to non-diarrheal sequelae including
64 "environmental enteric dysfunction (EED)," a condition characterized by impaired nutrient
65 absorption, impaired growth[7,8] and malnutrition,[9,10] adding significantly to the morbidity as well as
66 deaths from diarrhea and other infections[11]. The risk of stunting multiplies with each episode of
67 diarrheal illness in children under the age of two years[12], a period during which children residing in
68 impoverished areas commonly sustain multiple ETEC infections[8]. However, the molecular
69 pathogenesis underlying the intestinal changes associated with EED, and the contribution of
70 individual pathogens including ETEC remain poorly understood.

71 Similarly, toxin-producing *E. coli* have also been repeatedly identified in patients with tropical
72 sprue[13-15], a condition classically described in adults residing for extended periods of time in areas
73 where ETEC diarrheal disease is common. Like EED, tropical sprue is associated with changes to the
74 small intestinal villous architecture, including ultrastructural alteration of the epithelial brush border
75 formed by the microvilli[16,17], nutrient malabsorption, and wasting.

76 The basic molecular mechanisms underpinning acute watery diarrhea caused by ETEC are well-
77 established[18]. ETEC produce heat-labile (LT) and/or heat-stable (ST) enterotoxins that activate
78 production of cAMP and cGMP second messengers respectively, leading to activation of cellular
79 kinases that in turn modulate the activity of sodium and chloride channels in apical membrane of
80 intestinal epithelial cells to promote net efflux of salt and water into the intestinal lumen resulting in
81 watery diarrhea.

82 LT and cholera toxin (CT) share ~85 % amino acid identity, and both toxins exert their major
83 effects on the cell through the ADP-ribosylation of the alpha subunit of Gs (Gsα), a stimulatory
84 intracellular guanine nucleotide-binding protein. Inhibition of Gsα GTPase activity leads to
85 constitutive activation of adenylate cyclase and increased production of intracellular cAMP[19].

86 In its central role as a second messenger, cAMP governs a diverse array of cellular processes[20]
87 and modulates transcription of multiple genes through a number of cAMP-responsive transcriptional
88 activators and repressors[21] . cAMP activates protein kinase A (PKA), a heterotetramer, by liberating
89 its two regulatory subunits from the catalytic subunits which are then free to phosphorylate a wide
90 variety of cytoplasmic and nuclear protein substrates[22]. PKA largely regulates transcription by
91 phosphorylation of transcription factors including the cyclic AMP response element binding protein
92 (CREB) and the cAMP-response element modulator (CREM) which bind cAMP response elements
93 (CRE) in the promoter regions of target genes[21-23].

94 Notably, cholera toxin (CT), LT, and dibutyryl-cyclic AMP all induce hypersecretion and impact the
95 architecture of gastrointestinal epithelia in rodent small intestine [24], while small intestinal biopsies of
96 patients with acute cholera exhibit marked changes in the ultrastructure of the intestinal brush
97 border, the major absorptive surface in the small intestine[25,26], including shortening and disruption

98 of the microvilli. Consistent with these observations, studies of young children less than two years of
99 age in Bangladesh have specifically associated LT-producing ETEC with undernutrition[27], suggesting
100 that heat-labile toxin may exert effects on intestinal mucosa that extend beyond acute diarrheal
101 illness.

102 Here we demonstrate that in addition to the canonical effects of LT on cellular export of salt and
103 water into the intestinal lumen, this toxin impacts multiple genes involved in formation of microvilli,
104 resulting in marked alteration of the architecture of the intestinal brush border, the major site of
105 nutrient absorption in the small intestine. These effects are compounded by alteration of solute
106 transporters within the brush border epithelia, potentially disrupting the absorption of multiple
107 essential nutrients.

108 Results

109 heat-labile toxin markedly alters the transcriptomes of intestinal epithelial cells.

110 Commensurate with the importance of cAMP as a second messenger, we found that compared to
111 either untreated controls or cells treated with a catalytically inactive (E211K) mutant of LT, wild type
112 LT holotoxin substantially modulated transcription of many genes in intestinal epithelial cells. In
113 RNAseq studies of polarized Caco-2 intestinal epithelial cells we found that 3,832 genes were
114 significantly ($p \leq 10^{-5}$) upregulated and 3687 downregulated in response to LT, while binding of the
115 inactive toxin failed to induce significant changes in the transcriptome (figure 1a). However, Caco-2
116 cells are derived from distant metastases of a colon cancer tumor in which transcriptomes would
117 likely be altered relative to untransformed intestinal epithelia[28,29], and cAMP signaling is known to be
118 aberrant in some transformed cells[23]. Therefore, to examine a more physiologically relevant target,

119 we next examined the impact of LT on differentiated small intestinal enteroids. Here, we found that
120 far fewer genes were differentially expressed ($\leq 10^{-5}$) with 746 significantly upregulated, and 561
121 downregulated in response to intoxication with LT (figure 1b). Notably, however we found
122 substantial statistically significant overlap in genes significantly modulated in Caco-2 cells and
123 enteroids (supplemental table 3, supplemental dataset 1) with the transcription of hundreds of
124 genes significantly up- or down-regulated in both groups. Gene ontology enrichment analysis as
125 well as ontology-independent investigation of genes (CompBio, supplemental figure 1) modulated
126 by the toxin highlighted multiple cellular components associated with both the development and
127 function of the absorptive surface of the small intestine (supplemental dataset 2).
128

129 **heat-labile toxin impairs development of small intestinal microvilli.**

130 Small intestinal enterocytes are each covered with hundreds of microvilli, complex structures
131 comprised of a central core of actin filaments within protrusions of the plasma membrane.
132 Collectively, the luminal surface of the intestine formed by these microvilli, known as the brush
133 border, represents the major absorptive surface of the gastrointestinal tract. Three major classes of
134 proteins are required for the biogenesis of microvilli[30] (figure 2a). These include (1) proteins such as
135 villin, epsin, plastin, and EPS8 that bundle parallel clusters of actin filaments; BAIP2L1 (IRTKS)
136 responsible for recruiting the EPS bundling protein to the tips of microvilli[31]; (2) ezrin, myo1a[32],
137 myo6 that link the actin cytoskeleton with the plasma membrane; and (3) protocadherin molecules
138 CDHR2 and CDHR5 engaged in extracellular heterotypic complexes between the tips of the
139 microvilli[30] that are stabilized by a tripartite complex of MYO7B, ANKS4B[33], and USH1C[33].

140 Interrogation of transcriptional profiles indicated that the transcription of each of these classes of
141 genes was significantly altered following exposure to wild type heat-labile toxin (figure 2b). Similarly,
142 RT-PCR confirmed decreased expression of multiple genes involved in microvilli biogenesis,
143 including VIL1 encoding villin (figure 3a), and we were able to demonstrate that production of villin
144 was depressed in polarized small intestinal enteroids (figure 3b). In addition, TEM images of
145 polarized small intestinal enteroids exposed to heat-labile toxin demonstrated significantly
146 shortened and disorganized microvillus structures on the apical surface of enterocytes (figure 3c).

147 **heat-labile toxin modulates the transcription of multiple brush border nutrient transport**
148 **genes.**

149 The human solute carrier (SLC) gene superfamily is comprised of more than 50 gene families
150 thought to encode more than 300 functional transporters[34]. Many of the SLC proteins are enriched in
151 the small intestinal brush border where they transport critical nutrients including amino acids,
152 oligopeptides, sugars, and vitamins. We found that transcription of many SLC genes was altered in
153 Caco-2 cells as well as small intestinal enteroids (figure 4a). These included transporters for Zinc,
154 known both to be deficient in children with enteropathy[35], and a micronutrient critical for intestinal
155 homeostasis. Likewise transcription of SLC19A3 encoding the principal SLC responsible for uptake
156 of the water-soluble B vitamin thiamine (vitamin B1)[36] by differentiated intestinal epithelial cells lining
157 the surface of intestinal villi of the proximal small intestine[37,38](figure 4b) was repressed. Moreover,
158 we found that LT treatment of human small intestinal organoids also interfered with transcription of
159 the cis regulatory element specificity protein 1 (SP-1) previously shown to govern the transcription of
160 SLC19A3[39-41]. Finally, we found that thiamine transport was significantly depressed following

161 exposure to LT (figure 4c) providing additional evidence that ETEC can impair transport of critical
162 nutrients.

163 **LT-producing ETEC disrupt the absorptive architecture of the small intestine**

164 To further study the potential impact of ETEC toxins on the intestinal architecture, we performed
165 challenge studies in infant mice. Compared to sham-challenged (PBS) controls, or mice challenged
166 with a toxin deficient strain of ETEC, we again noted down-regulation of genes involved in F-actin
167 bundling, membrane cross-linking, and intermicrovillus adhesion complex formation, all required for
168 intestinal microvilli (figure 5a) biogenesis. Likewise, on examination of small intestinal villi we found
169 that production of villin in enterocyte brush borders was substantially decreased relative to sham
170 challenged controls (figure 5b-d). In mice challenged with a wild type ETEC isolate that makes ST
171 and LT, but not a LT/ST-toxin-negative mutant (jf4763, supplemental table 1), we observed
172 significant alteration in architecture of the intestinal brush border with significant shortening and
173 disorganization of the microvilli (figure 5e,f; supplemental figure 2a-d) reminiscent of the earlier
174 ultrastructural studies of patients with tropical sprue [17] and *V. cholerae* infections[25]. Similarly, we
175 found that in mice challenged with a strain containing an isogenic mutation in *eltA* (jf571,
176 supplemental table 1) encoding the LT A subunit, which still makes heat-stable toxins, the microvillus
177 architecture was preserved (figure 5g, h), suggesting that LT is the principal toxin underlying the
178 enteropathic changes to the enterocyte surfaces. However, despite the dramatic toxin-dependent
179 changes to the absorptive surface of the intestine, the growth kinetics of suckling mice challenged
180 with either wild type bacteria or toxin deletion mutants were surprisingly similar (supplemental figure
181 3a,b) and paralleled those of sham challenged controls, suggesting that other elements including

182 caloric restriction, and alterations in gut microbiota may be required to replicate growth faltering
183 observed in children[42].

184 **maternal vaccination with LT prevents brush border disruption**

185 To address whether enteropathic changes to the small intestine can be prevented by vaccination,
186 and to further define the role of LT, we vaccinated mouse dams with heat-labile toxin and examined
187 the brush border ultrastructure in suckling mice. Vaccinated dams but not sham vaccinated controls
188 expressed significant levels of IgA and IgG in breast milk (figure 6a), consistent with increased levels
189 of antibodies in the stomachs of infant mice (figure 6b). Notably, we found that maternal vaccination
190 with LT completely abrogated changes to the microvilli (figure 6c,d) further substantiating the
191 importance of LT in driving changes to the epithelial architecture.

192 **LT modulates key transcription factors that govern enterocyte development**

193 Despite the marked alteration in transcription mediated by LT the majority of genes critical for
194 brush border development lacked conserved CRE sites [23]. Therefore, we performed transcription
195 factor target enrichment analysis[43,44] to identify potential transcription factors responsible for
196 differential regulation of genes significantly ($P < 0.05$) upregulated or downregulated by LT in both
197 Caco-2 and enteroid RNA-seq datasets (supplemental table 4, supplemental dataset 1). The
198 upregulated genes were most significantly ($p = 4.2 \times 10^{-3}$) linked to transcription factor targets of AP-
199 1 encoded by the *c-jun* gene, previously shown to be regulated by cAMP[45], and to be involved in
200 intestinal epithelial repair[46]. Notably however, downregulated genes were most significantly
201 enriched in targets for the HNF4α transcription factor or its intestine specific paralog HNF4γ ($P =$
202 1.9×10^{-4}) that were recently shown to regulate multiple genes required for brush border

203 development[47,48]. Importantly, PKA has also been shown to phosphorylate HNF4 α at a consensus
204 recognition site within the DNA binding domain, shared with HNF4 γ, inhibiting transcription[49].
205 Of note, the transcription of both paralogs was found to be significantly depressed following
206 exposure of intestinal epithelia to LT (figure 7A,B), as were levels of HNF4γ in nuclear fractions from
207 toxin-treated cells (figure 7C), suggesting that activation of cAMP can interfere with transcription
208 mediated by HNF4. To further examine the impact of LT on HNF4-mediated transcription we
209 introduced a transcriptional reporter plasmid containing 6 tandem copies of the HNF4
210 transcriptional response element (5'- CAAAGGTCA-3') linked to a human codon optimized *Gaussia*
211 *princeps* luciferase into Caco-2 cells. These assays demonstrated that HNF4-mediated transcription
212 was dramatically reduced in cells treated with LT (figure 7D). Similarly, we found that relative to
213 nuclei of intestinal epithelia cells in ileal segments from sham-challenged control mice, those from
214 ETEC-challenged mice exhibited significantly less HNFγ (figure 7E) further supporting a role for
215 ETEC in modulating the production of this important transcription factor. Chen, *et al* described a
216 "feed-forward regulatory module" essential to enterocyte differentiation in which HNF4 and SMAD4
217 transcription factors reciprocally activate each other's transcription. As would be predicted from this
218 model, we found that transcription of SMAD4 was also impaired by LT (supplemental figure 4A),
219 leading us to propose a model in which LT mediates phosphorylation of HNF4 by PKA, interrupting
220 this critical transcription module (Supplemental figure 4B-D).
221 Collectively, the current studies demonstrate that in addition to their known canonical effects on
222 ion transport that culminate in watery diarrhea, ETEC toxins can drive appreciable derangement of
223 enterocyte architecture and function by interfering with key pathways in intestinal epithelia that
224 govern the formation of mature enterocytes capable of effective nutrient absorption. These findings

have important implications for our understanding and prevention of enteropathic conditions linked to ETEC.

228 ## Discussion

229 Understanding the molecular events that lead to sequelae of undernutrition and growth faltering
230 following ETEC infections may be key to the effective design of prevention strategies including
231 vaccines[50]. Although the molecular mechanisms involved in the fluid and ion fluxes into the intestinal
232 lumen leading to diarrhea are firmly established, only recently has evidence emerged to suggest
233 that ETEC toxins may incite previously unappreciated changes in small intestinal epithelia[51,52]. The
234 present studies, initiated to identify additional effects of LT, were prompted by an appreciation that
235 cyclic nucleotides, particularly cAMP, govern a multitude of cellular pathways potentially resulting in
236 collateral impacts that extend beyond the acute episodes of diarrhea. Consistent with this model, we
237 found that exposure of intestinal cells to heat-labile toxin altered the transcription of hundreds of
238 genes. A central theme highlighted in the analysis of these transcriptional alterations is that LT
239 affects major classes of genes involved in biogenesis of microvilli and function of the intestinal brush
240 border, the major site of nutrient uptake in the small intestine, potentially offering a direct molecular
241 link to sequelae of malnutrition and impaired growth in children.

242 The potential clinical relevance of the observations reported here is highlighted by remarkably
243 similar ultrastructural alteration of intestinal epithelial cells seen in small intestinal biopsies of
244 patients with acute cholera[25] and tropical sprue[17]. In both entities, the brush border was noted to be
245 abnormal, with shortened, irregular microvilli. Importantly, however despite the structural and
246 functional similarity between LT and CT, clinical cholera, unlike ETEC infections, has not been linked
247 to enteropathy or attendant sequelae. Whether this relates to the repetitive nature of ETEC
248 infections compared to the durable protective immunity that follows a single *V. cholerae* infection[53]
249 is not presently clear. Similarly, while tropical sprue remains a leading cause of malabsorption in

250 regions where infectious diarrhea is prevalent[54-56], the most debilitating forms of this illness have not
251 typically followed isolated cases of traveler's diarrhea, but occur in resident populations or
252 expatriates[57] repeatedly assailed by diarrhea while residing in endemic regions[58].
253 The negative impacts of LT on brush border architecture with commensurate reduction in surface
254 area available for nutrient absorption, are compounded by the alteration of multiple SLC genes that
255 encode transporters critical for uptake of essential vitamins and other molecules. Importantly, small
256 intestinal biopsies obtained from Zambian children with enteropathy and refractory stunting
257 exhibited similar changes in SLC gene expression profiles[59]. The decreased transcription of
258 molecules required for intestinal zinc uptake, in cells treated with LT is particularly intriguing given
259 the known aberrations in zinc absorption in children with enteropathy[35,60,61], the possible
260 contribution of zinc deficiency to enteropathic changes[62], and the salutary effects of zinc in treatment
261 of children with diarrhea[63,64].
262 Further study will be needed to precisely delineate the role of ETEC LT and ST enterotoxins, alone
263 and in combination, in driving enteropathic changes to the intestine and sequelae. ST-producing
264 ETEC were most strongly associated with moderate to severe diarrhea in GEMS[3], and follow-on
265 studies of children enrolled in these studies have also linked infections with ETEC encoding heat-
266 stable toxin to growth faltering[7]. However, our earlier analysis of a global collection of more than
267 1100 ETEC isolates, including those collected in GEMS, demonstrated that slightly more than half of
268 all ST-encoding strains also encoded LT, and that roughly one third of the isolates overall encoded
269 LT alone, ST-LT, or ST only[65]. While LT-producing ETEC have been specifically linked to malnutrition
270 among children in Bangladesh[27], and our *in vitro* and animal studies point to the potential
271 importance of LT, additional effort will be needed to correlate toxin-induced morphologic and

272 functional perturbation of the intestinal brush border with outcomes in children. Importantly, the
273 long-term morbidity associated with ETEC infections does not appear to correlate with the severity
274 of diarrhea as both mild illness[4], and perhaps asymptomatic colonization may lead to growth
275 faltering.

276 Further refinement of animal models that can faithfully recapitulate features of enteropathy are
277 also needed. Despite marked derangement of the brush border following infection, single infections
278 of neonatal mice did not lead to sustained growth defects suggesting it may be difficult to
279 completely capture the full effects of ETEC in a small animal model. Indeed, conventional mice lack
280 genes that could be required to reproduce the full effects of ETEC. For instance, each of the
281 carcinoembryonic antigen cell adhesion molecules (CEACAMs) that are substantially upregulated on
282 human small intestinal epithelia in response to LT, and which we have recently shown to play a
283 critical role in ETEC interactions with human small intestine[51], are absent in mice.

284 While the precise mechanism underlying LT-mediated modulation of genes required for
285 microvillus biogenesis and absorptive function of the brush border is presently unclear, stimulation
286 of adenylate cyclase invokes many cAMP-responsive nuclear factors that may serve either to activate
287 or repress transcription. Genes implicated in development of microvilli are mostly devoid of
288 consensus palindromic (TGACGTCA) or "half" (CGTCA) cAMP response element (CRE) sites within
289 their promoter regions for direct modulation by CREB[66], which typically is involved as a
290 transcriptional activator, and both CREB and CREM can yield several alternatively spliced variants
291 that may act as either activators or repressors[67]. cAMP second messaging also engages multiple
292 signaling pathways converging at CREB[68], and PKA can phosphorylate and modulate the activity of
293 multiple transcription factors to act either as transcriptional activators or repressors, including SP1[69].

294 Notably, putative binding sites for HNF4, a cAMP-modulated transcription factor[49] known to regulate
295 genes needed for formation of microvilli[47,48], were significantly enriched in the promotors of genes
296 downregulated by LT. Both HNF4α and HNF4γ possess canonical PKA recognition sites within their
297 DNA binding motifs, and PKA phosphorylation of these sites interrupts transcription[70]. HNF4
298 activates the transcription of SMAD4, and in turn SMAD4 activates transcription of HNF4[71]. Both
299 transcription factors then engage genes needed for effective differentiation of stem cells to mature
300 enterocytes[71]. Modulation of the activity of this transcription factor by LT would therefore be
301 predicted to have a marked impact on pathways critical to intestinal epithelial homeostasis.
302 We should also note that increases in cellular cAMP can impact multiple cellular pathways
303 independent of PKA. Included among these are pathways governed by a more recently discovered
304 family of cellular cAMP-binding molecules, exchange proteins activated by cAMP (EPACs). EPACs
305 appear to play critical roles as guanine exchange factors that regulate GTPase proteins[72] and are in
306 involved in complex signaling networks implicated in cell growth, differentiation, and
307 morphogenesis[73,74].
308 cAMP can also exert potent epigenetic influences on transcription. CREB-binding protein (CBP)
309 possesses intrinsic histone acetyl-transferase (HAT) activity[75], and can therefore modulate chromatin
310 remodeling, enhancing access of transcription factors. In addition, cAMP messaging through PKA
311 leads to phosphorylation-dependent activation of the histone demethylase enzyme PHF2 to
312 promote the transcription of multiple genes that can impact transition from stem cells to epithelial
313 cells[76].
314 Altogether it seems likely that multiple pathways governed by increases in cellular cAMP may
315 underlie the morphologic and functional disruption of the brush border epithelial observed in our

316 studies. Nevertheless, the data presented here provide compelling evidence that the heat-labile
317 toxin of ETEC ultimately impacts multiple genes required for the biogenesis and function of the
318 brush border, the major site of nutrient absorption in the human small intestine. The findings may
319 have significant implications for our understanding of sequelae linked to ETEC including
320 environmental enteropathy in young children, and tropical sprue in adults. The increased
321 acknowledgement of long-term morbidity linked to ETEC and an improved understanding of the
322 role of ETEC enterotoxins as drivers of this morbidity may also strengthen the case for vaccines[50]
323 specifically engineered to prevent both the acute illness and sequelae.
324

325 ## Methods

326 ### Culture and differentiation of Enteroids

327 Biopsy samples from adult patients undergoing routine endoscopy were obtained at Washington
328 University School of Medicine after patient consent and approval from the Institutional review board.
329 Purified crypt cells from the ileum were re-suspended in Matrigel (BD Bisosciences, San Jose,
330 California, USA) and 15 µL of re-suspended matrix gel was added to each well in 24 well plates.
331 Plates were incubated at 37° C and 5% CO2 with 50% L-WRN conditioned media (CM) and 50%
332 primary culture medium (Advanced DMEM/F12, Invitrogen) supplemented with 20% FBS, 2 mM L-
333 glutamine, 100 units/mL penicillin, 0.1 mg/mL streptomycin, 10 µM Y-27632 (ROCK inhibitor, Tocris
334 Bioscience, R&D systems, Minneapolis, MN, USA), and 10 µM SB431541 (TGFBR1 inhibitor, Tocris
335 Bioscience, R&D systems).
336 To induce differentiation and polarization of enteroids, cells were washed once to remove
337 Matrigel, followed by trypsinization and centrifugation at 1100 x g for 5 minutes. Cells were then re-
338 suspended in 1:1 CM and primary medium with Y-27632 and SB431541 as described above. Cells
339 were then plated on semiporous filters (Transwells®, 6.5 mm insert, 24 well plate, 0.4 µm polyester
340 membrane, Corning Incorporated, Kennebunk, ME, USA) that had been previously coated with
341 Collagen IV (Millipore Sigma). Transwell® inserts were rinsed with DMEM/F12 with Hepes, 10% FBS,
342 L-glutamine, Penicillin, and streptomycin. Cells were allowed to grow to confluency in 50%
343 conditioned media (CM) and then changed to differentiation medium (5% CM in primary medium +
344 ROCK inhibitor) for 48 hours. Differentiated cells were used for toxin treatment.

345 **propagation of Caco-2 cells**

346 Caco-2 intestinal epithelial cells were obtained from ATCC (ATCC HTB-37) and cultured at 37 °C, 5%
347 CO_2, in Eagle's MEM supplemented with 20% of fetal bovine serum (FBS). To generate polarized
348 monolayers, ~1 x10^5 cells were seeded onto polystyrene membrane filters (0.4μM, 6.5mm diameter
349 insert, Transwell, Corning) and grew for at least a week prior to toxin treatment. Media was replaced
350 with fresh media every two days.

351 **Toxin treatment**

352 Polarized differentiated cells were treated with heat-labile toxin (LT) in differentiation medium
353 (100 ng/mL) in a volume of 700 μL at the basolateral side of the Transwell insert and 100 μL volume
354 on the apical aspect of the monolayer. Treated cells were incubated at 37° C for 18 hours and then
355 fixed for transmission electron microscopy or fluorescence microscopy, or lysed for RNA extraction
356 (GE Healthcare, Buckinghamshire, UK).

357 **RNA extraction and cDNA synthesis**

358 RNA was extracted using Illustra RNAspin Mini RNA extraction kit (GE Healthcare,
359 Buckinghamshire, UK). Three biological replicates per treatment (untreated and LT treated) were
360 submitted to Genome Technology Access Center (GTAC) at Washington University in St. Louis
361 School of Medicine for RNA-seq library preparation. An Agilent Bioanalyzer was used to determine
362 the integrity of RNA samples. cDNA was generated using Superscript™ Vilo™ cDNA synthesis kit
363 (Invitrogen by Thermo Fisher) after normalizing RNA concentrations.

364 **RNA-seq Library Preparation**

365 Library preparation was performed with 10 ng of total RNA, integrity was determined using an
366 Agilent bioanalyzer. ds-cDNA was prepared using the SMARTer Ultra Low RNA kit for Illumina
367 Sequencing (Clontech) per manufacturer's protocol. cDNA was fragmented using a Covaris E220
368 sonicator using peak incident power 18, duty factor 20%, cycles/burst 50, time 120 seconds. cDNA
369 was blunt ended, had an A base added to the 3'ends, and then had Illumina sequencing adapters
370 ligated to the ends. Ligated fragments were then amplified for 12-15 cycles using primers
371 incorporating unique index tags. Fragments were sequenced on an Illumina HiSeq-2500 using
372 single reads extending 50 bases.

373 **RNA-seq data processing and analysis**

374 RNA-seq reads were aligned to the Ensembl top-level human genome assembly with STAR
375 version 2.7.3a. Gene counts were derived from the number of uniquely aligned unambiguous
376 reads by Subread:featureCount version 1.54.1. Read counts were used as input for DESeq2
377 differential gene expression analysis (version 1.24.0)[77] with default settings, and a minimum *P*-value
378 significance threshold of 10^{-5} (after False Discovery Rate [FDR[78]] correction for the number of tests).
379 Fragments per kilobase per million reads mapped (FPKM) values for relative gene expression were
380 calculated from DESeq2-normalized read counts, and Z-scores were calculated per gene using the
381 average and standard deviations of FPKM values across samples. Log_2 fold changes were identified
382 from DESeq2 differential expression output. Pathway enrichment analysis for KEGG[79] and Gene
383 Ontology (GO)[80] pathways among gene sets of interest was performed using the over-

384 representation analysis tool provided on the WebGestalt[43] web server (version 2019). Heatmap and
385 bar graph visualization was performed with Microsoft Excel.
386 Transcript counts were produced by Sailfish version 0.6.3. Sequencing performance was
387 assessed for total number of aligned reads, total number of uniquely aligned reads, genes and
388 transcripts detected, ribosomal fraction known junction saturation and read distribution over known
389 gene models with RSeQC version 2.3.
390 All gene-level and transcript counts were then imported into the R/Bioconductor package EdgeR
391 and TMM normalization size factors were calculated to adjust for samples for differences in library
392 size. Ribosomal features as well as any feature not expressed in at least the smallest condition size
393 minus one sample were excluded from further analysis and TMM size factors were recalculated to
394 created effective TMM size factors. The TMM size factors and the matrix of counts were then
395 imported into R/Bioconductor package Limma and weighted likelihoods based on the observed
396 mean-variance relationship of every gene/transcript and sample were then calculated for all samples
397 with the voomWithQualityWeights function. Performance of the samples was assessed with a
398 spearman correlation matrix and multi-dimensional scaling plots. Gene/transcript performance was
399 assessed with plots of residual standard deviation of every gene to their average log-count with a
400 robustly fitted trend line of the residuals. Generalized linear models were then created to test for
401 gene/transcript level differential expression. Differentially expressed genes and transcripts were
402 then filtered for FDR adjusted p-values less than or equal to 0.05.
403 The biological interpretation of the large set of features found in the Limma results were then
404 elucidated for global transcriptomic changes in known Gene Ontology (GO) and KEGG terms with
405 the R/Bioconductor packages GAGE and Pathview. Briefly, GAGE measures for perturbations in GO

406 or KEGG terms based on changes in observed log_2 fold-changes for the genes within that term
407 versus the background log_2 fold-changes observed across features not contained in the respective
408 term as reported by Limma. For GO terms with an adjusted statistical significance of FDR <= 0.05,
409 heatmaps were automatically generated for each respective term to show how genes co-vary or co-
410 express across the term in relation to a given biological process or molecular function. In the case of
411 KEGG curated signaling and metabolism pathways, Pathview was used to generate annotated
412 pathway maps of any perturbed pathway with an unadjusted statistical significance of p-value <=
413 0.05. Genes significantly modulated in both Caco-2 cells and enteroids were subjected to further
414 ontology-free analysis via CompBio v1.4 (PercayAI, Inc., www.percayai.com/compbio)[81] to identify
415 unifying biological themes in sets of genes differentially expressed between pairwise comparisons of
416 different groups.
417

418 **Quantitative real time PCR**

419 Quantitative real time PCR was performed using a QuantStudio 3 real-time detection system
420 (Applied Biosystems). Fast SYBR Green master mix (Applied Biosystems / Thermo Fisher) was used
421 for qPCR analysis. Disassociation curve analysis was performed to assess the specificity of
422 amplification for each sample, and PCR product size was verified by agarose gel electrophoresis.
423 Percent expression was normalized by GAPDH and analyzed using the comparative threshold cycle
424 (Ct) method. Amplification of SLC19A3 transcripts from small intestinal enteroids was performed as
425 recently described[82] with relative gene expression normalized to β actin. HNF4a, HNFg, and SMAD4

426 gene expression was determined by TaqMan (ThermoFisher) using validated primer and probe sets.
427 Primers and TaqMan probes used in this study are listed in Supplemental Table 2.

428 **HNF4 transcriptional reporter assays**

429 To assess the impact of LT on HNF4-mediated transcription, pTR104 (GeneCopoeia) carrying 6
430 copies of the HNF4 transcriptional response element upstream of a secreted *Gaussia* luciferase
431 (Gluc) reporter gene was transfected (FuGENE, Promega) into confluent Caco-2 cells. Media (EMEM,
432 ATCC) were exchanged 24 hours after transfection, and after an additional 24 hours baseline
433 samples of media were removed from each well and stored at -80°C. Wells were then treated with
434 heat labile toxin (100 ng/ml) overnight (16 hours). At the end of treatment cell culture supernatants
435 media were transferred to black walled microplates (Greiner 655086) and processed as directed
436 (Secrete-Pair Luminescence, GeneCopoeia, Inc. Rockville, MD), followed by luminescence detection
437 (Synergy H1, BioTek). Data are expressed as Relative Light Units (RLU) before and after treatment
438 with LT.

439 **Thiamin Uptake**

440 Initial rates (30 min; at 37 °C) of carrier-mediated thiamin uptake were examined in LT-treated (100
441 ng/ml; overnight) and untreated control differentiated small intestinal enteroid monolayers
442 incubated in Krebs–Ringer buffer (pH 7.4) containing [^{3}H]-thiamin (15 nM). Enteroid monolayers
443 were then washed with ice-cold Krebs–Ringer buffer followed by lysis with NaOH and neutralization
444 with 10 N HCl. The radioactive content was counted using a liquid scintillation counter as described
445 previously[82]. Uptake of thiamin by its respective and distinct carrier-mediated mechanism was
446 determined by subtracting uptake of [^{3}H]-thiamin in the presence of a high pharmacological

447 concentration (1 mM) of unlabeled thiamin from uptake in their absence; all uptake data points were
448 calculated relative to total protein content (in milligrams) of the different preparations and presented
449 as percentage relative to simultaneously performed controls.

450 **confocal microscopy**

451 Cell monolayers were fixed with 2% paraformaldehyde for 30 min at 37 °C and then washed 3× with
452 PBS prior to blocking with 1% BSA in PBS for 1 h at room temperature. Villin expression was
453 detected using 1:100 dilution of anti-villin antibodies raised in mice (Santa Cruz Biotechnology) for 1
454 hour at room temperature followed by additional 1 hour incubation with 1:200 dilution of
455 fluorescence-tagged goat anti-mouse IgG Alexa Fluor 488 (Thermofisher) (Supplemental Table 5).
456 Cell membranes were stained with 1:2000 dilution of CellMask orange (Invitrogen) and nuclei were
457 counterstained with DAPI (1:1000) and mounted on glass slides using Prolong Gold antifade reagent
458 (Invitrogen). Images were captured and analyzed on a Nikon C2 confocal microscope equipped with
459 NIS-Elements AR 5.11.01 software (Nikon).

460 **electron microscopy**

461 For ultrastructural analyses, *in vitro* grown differentiated polarized monolayers of human ileal
462 enteroid samples as well as mouse intestinal biopsy samples were fixed in 2%
463 paraformaldehyde/2.5% glutaraldehyde (Ted Pella, Inc., Redding, CA) in 100 mM sodium cacodylate
464 buffer, pH 7.2 for 2 hours at room temperature and then overnight at 4°C. Samples were washed in
465 sodium cacodylate buffer and postfixed in 2% osmium tetroxide (Ted Pella, Inc) 1 hour at room
466 temperature. Samples were then rinsed in dH_20, dehydrated in a graded series of ethanol, and
467 embedded in Eponate 12 resin (Ted Pella, Inc.). Sections of 95 nm were cut with a Leica Ultracut

468 UCT ultramicrotome (Leica Microsystems Inc., Bannockburn, IL), stained with uranyl acetate and lead
469 citrate, and viewed on a JEOL 1200 EX transmission electron microscope (JEOL USA Inc., Peabody,
470 MA) equipped with an AMT 8 megapixel digital camera and AMT Image Capture Engine V602
471 software (Advanced Microscopy Techniques, Woburn, MA). Images were analyzed using ImageJ
472 software for microvilli length and structures.
473

474 **identification of potential transcription factor target sites**

475 The CREB targets database[66] (http://natural.salk.edu/CREB/) was used to identify potential
476 categorical CRE full (TGACGTCA) or half (TGACG/CGTCA) sites within the promotor regions of
477 genes modulated by heat-labile toxin. Following previously described protocol[23], 5 kilobase
478 upstream sequences from each human gene were retrieved from Ensembl[83] and were searched for
479 the CREB binding sites TGACGTCA and TGACGTAA (and their reverse complements), based on
480 sequences retrieved from the TRANSFAC[84] database (matrix ID: V$CREB_01). CREB sequences
481 matches were identified in the upstream sequences of 1,302 genes. WebGestalt[85] was used for
482 overall functional enrichment of potential transcription factor binding sequences upstream from
483 genes that were significantly ($p<0.05$) up- and down-regulated in both Caco-2 cells and enteroids.
484

485 **suckling mouse challenge studies**

486 Studies in mice were performed under protocol 20-0438 approved by the Washington University
487 in Saint Louis Institutional Animal Care and Use Committee. In neonatal mouse challenge studies, 3-
488 day-old CD-1 mice were inoculated with wild type ETEC (H10407), isogenic toxin deletion mutants,

489 or sterile PBS (sham negative controls). Inocula were prepared from frozen glycerol stocks
490 maintained at -80°C grown overnight (~16 hours) in 2 ml Luria Bertani (LB) broth in a shaking
491 incubator (at 37°C, 225 rpm). Cultures were then diluted 1:100 in 20 ml of fresh LB, grown for
492 additional 2 hours, and bacteria harvested by centrifugation (6000 rpm, 5 minutes at 4°C). Pellets
493 were then washed once in ice-cold sterile PBS, then resuspended to a density of ~$1*10^5$ Colony
494 forming units (CFU) per 20 µl inoculum. CFU in each inoculum were determined by plating serial
495 dilutions LB-agar plates. Mice were then inoculated with ETEC directly into the stomach through the
496 abdominal wall using a 31g insulin needle. Following infection, mice were marked with tattoo ink to
497 define groups and returned to the cage. Seven days post infection mice were sacrificed, and the ileal
498 tissue collected fixed for microscopy, or preserved for RNA extraction.

499 **Vaccination and immunologic assessment**

500 Adult female mouse dams were vaccinated intranasally three times at 2-week intervals with 10 µg LT
501 holotoxin in PBS, with the last dose administered approximately 2 weeks prior to anticipated
502 delivery. Control mice were mock vaccinated with PBS. Fecal pellets collected from vaccinated dams
503 were used to assess mucosal responses to LT. To collect breast milk the dam was separated from the
504 litter ~2hours prior to milking. Oxytoxin (Sigma O3251), 0.002 IU/g, was injected IP to stimulate milk
505 production, followed by collection via pipette tip. Anti-LT immune responses in maternal fecal
506 extracts and breast milk, and stomach contents and sera of neonates were assessed by GM1
507 ganglioside[86] kinetic ELISA[87] for anti-LT IgA and IgG, using plates coated with GM1 (Sigma G7641),
508 as previously described[88].

509

510

Figures

figure 1

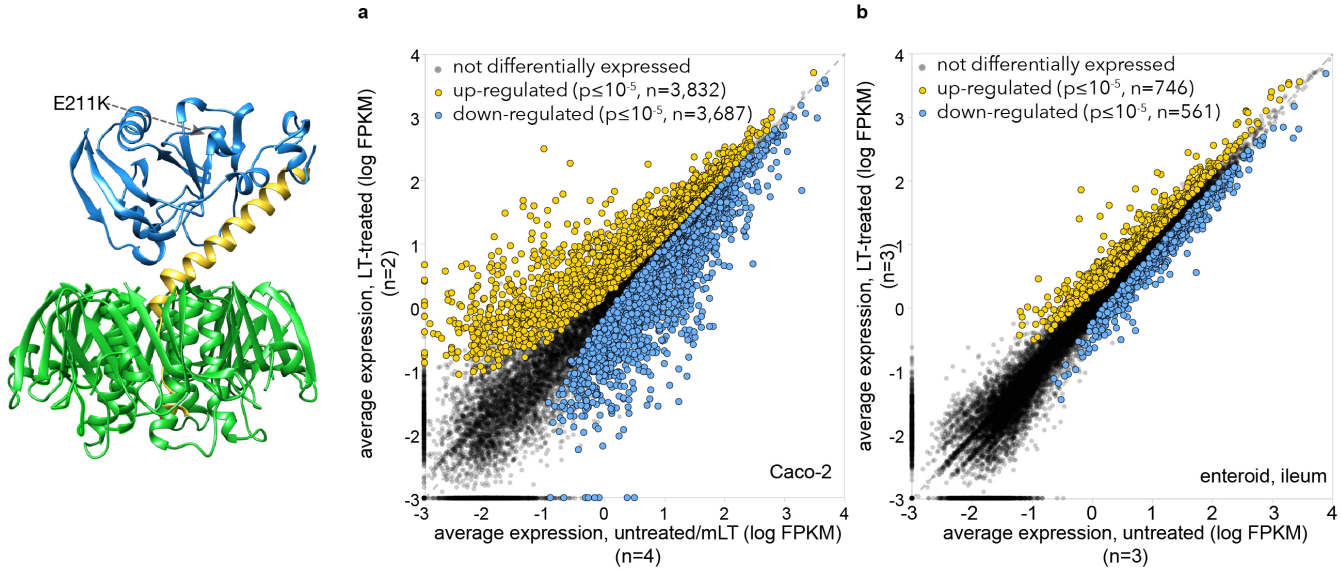

figure 1. Heat-labile toxin modulates expression of multiple genes in intestinal epithelia. Model at left depicts the *E. coli* heat-labile toxin[89] based on PDB structure 1LTS with the A1 subunit in blue the A2 region of in yellow and pentameric B subunit in green. The E211K mutation of mLT is in the active site of the A1 subunit. **A.** Scatterplot of RNAseq data right depicts differential expression profiles of Caco-2 cells following exposure to heat-labile toxin relative to untreated cells or cells treated with the biologically inactive mLT. **B.** RNAseq data from polarized small intestinal ileal enteroids treated with LT compared to control untreated cells.

figure 2

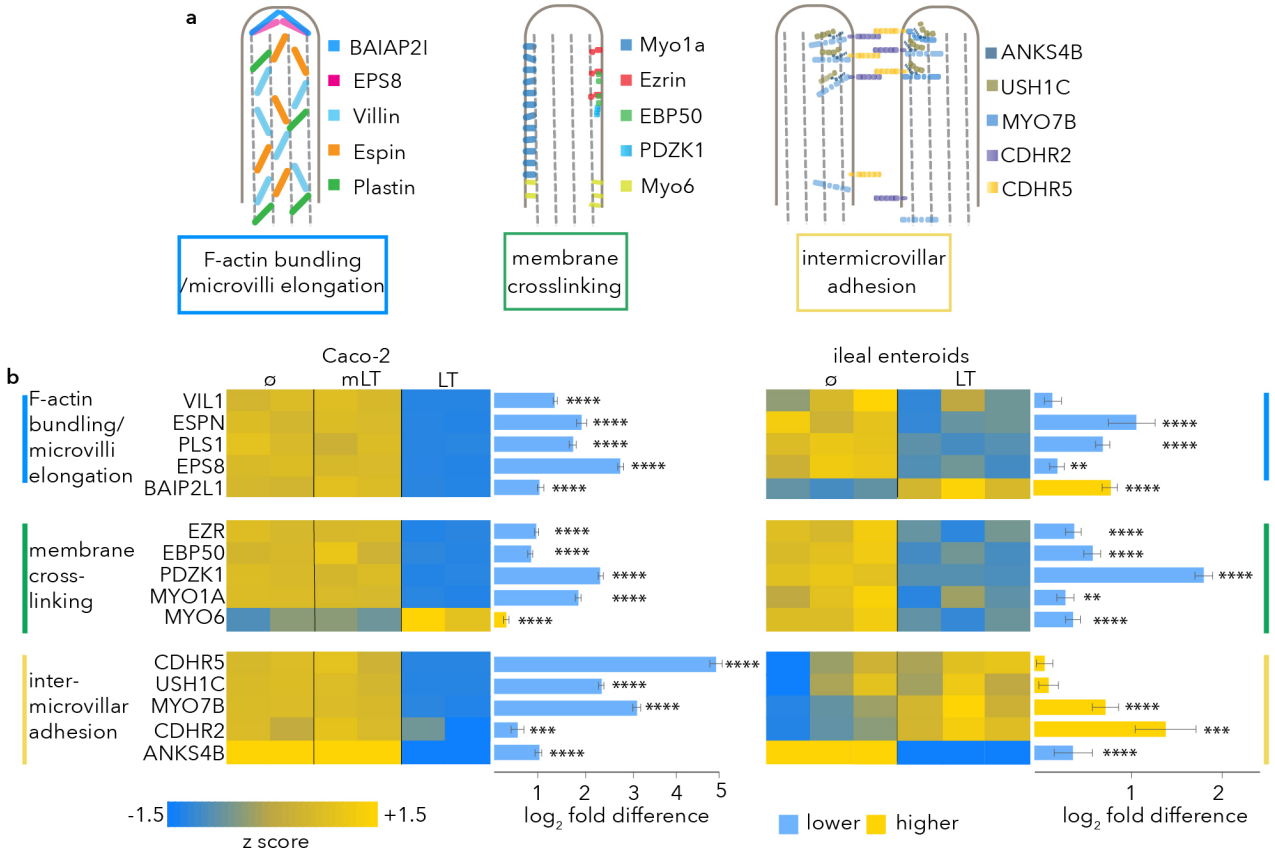

figure 2. heat labile toxin modulates multiple genes involved in microvillus assembly. **a.** diagram at top (adapted from reference[30]) depicts molecules involved in key elements of microvillus development. **b.** heat maps of RNAseq data obtained following treatment of Caco-2 intestinal cells (left) with mLT, or LT; and ileal enteroids (right) treated with LT relative to control untreated cells. RNAseq fold change data comparisons were made with DESeq2[90]. *p≤0.05, ** p≤0.01, *** p≤0.001, **** p≤10^{-4}, *****p≤10^{-5}.

figure 3

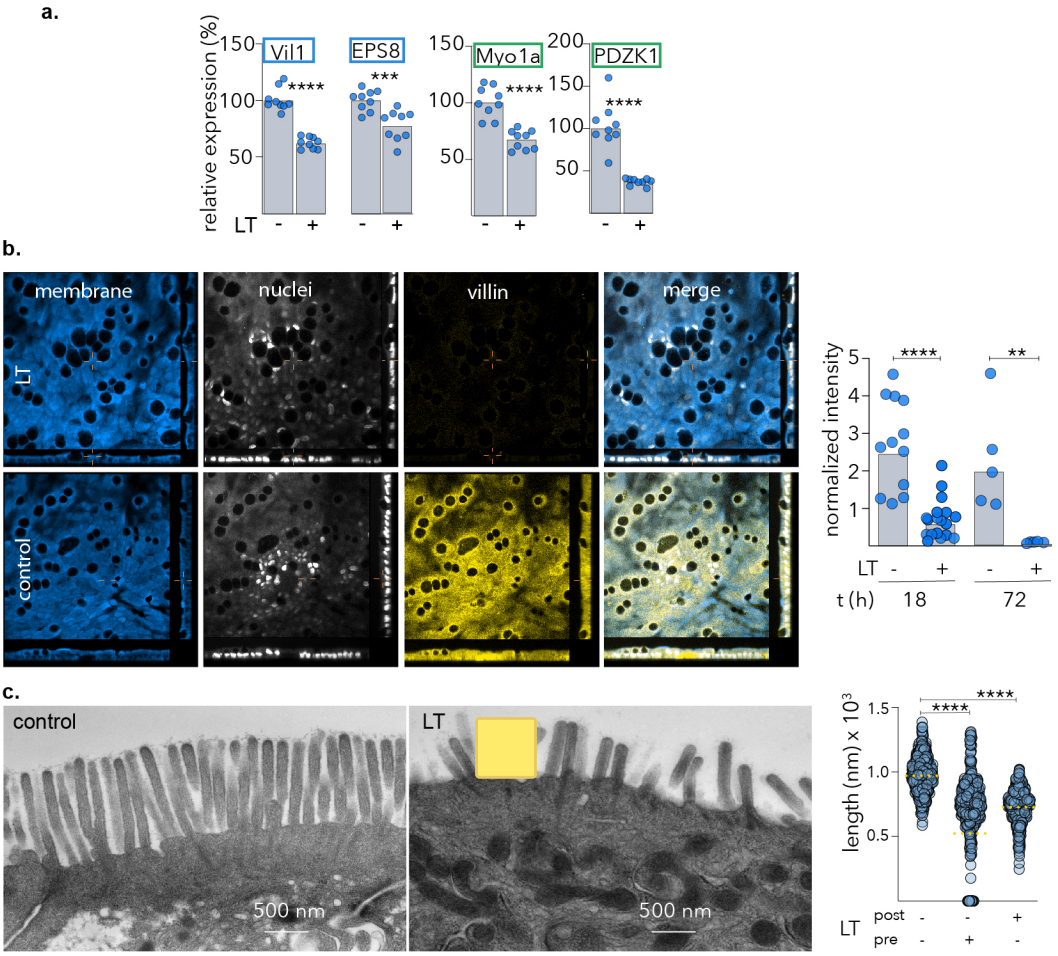

figure 3. heat labile toxin impairs effective formation of small intestinal microvilli.

a. quantitative RT-PCR data for selected microvillus genes comparing untreated (-) and LT-treated (+) ileal epithelial cells. **b.** Villin production is suppressed in small intestinal enteroids following treatment (t+72h) with LT . Shown are representative confocal images obtained showing membrane (CellMask, blue), villin (gold) nuclei (white), and merged image. Graph at right shows villin mean fluorescence intensity data normalized to the nuclear signal following overnight (~18 hours), and treatment for 72 hours. ****p<0.0001, **p=0.008, Mann-Whitney 2 tailed testing. **c.** TEM images of small intestinal microvilli following treatment LT (right) compared to control untreated cells (left). Graph at right shows length of microvilli when enteroids are treated before (pre) and after (post) differentiation on polarized ileal cells ****<0.0001 by ANOVA (Kruskal-Wallis, nonparametric testing).

551 **figure 4**

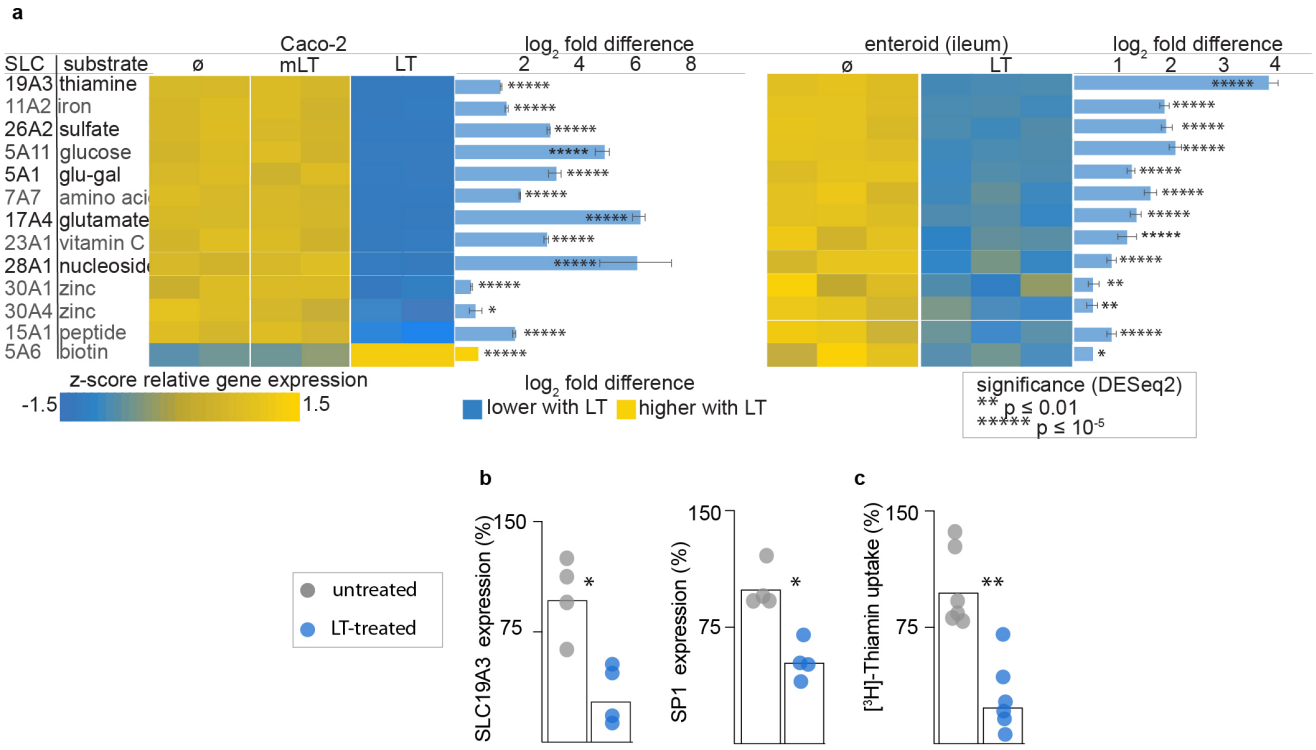

552

553 **figure 4. heat-labile toxin alters the transcription of multiple brush border SLC genes.**

554 **a.** heat-map indicating key SLC genes modulated by heat labile toxin (LT) compared to enzymatically

555 inactive E112K LT mutant (mLT), or untreated (ø) Caco-2 cells (left) and human small intestinal (ileal)

556 enteroids (Hu235D, right). **b.** qRT-PCR confirming LT-mediated modulation of genes in ileal

557 (Hu235D) enteroids encoding the major thiamine transporter SLC19A3 and the SP1 cis regulatory

558 element. Data reflect two independent experiments with 2 replicates each. **c.** uptake of [^{3}H]-thiamine

559 by Hu235 D cells is impaired following LT treatment. Data presented are from two independent

560 experiments with n=3 replicates each. (* <0.05, **<0.01 Mann-Whitney nonparametric comparisons).

561

562
563
564

figure 5.

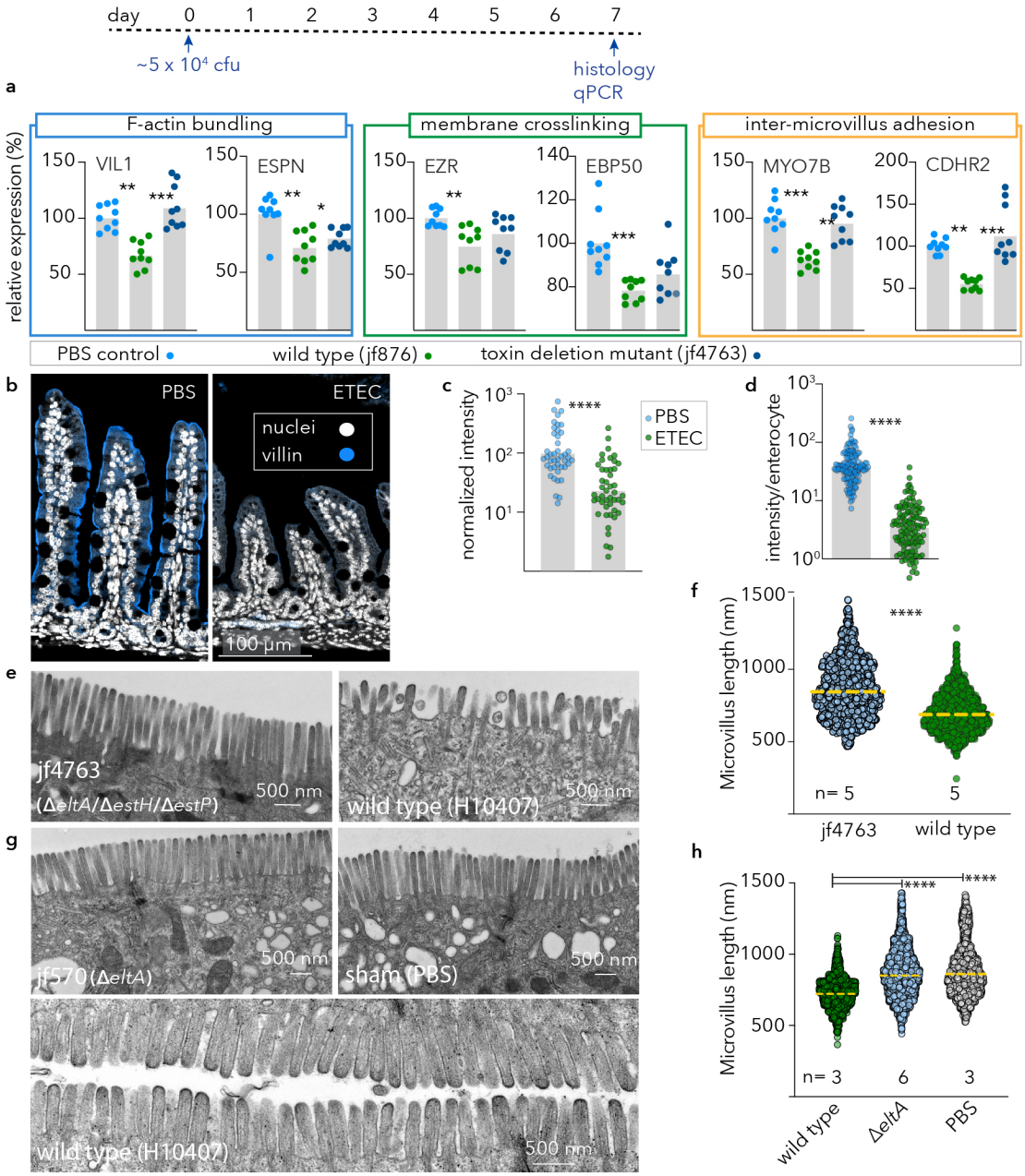

figure 5. ETEC disrupts *in vivo* formation of small intestinal microvilli

Timeline at top depicts challenge with ETEC or control nontoxigenic isolate, or sham (PBS) challenge. **a.** Quantitative PCR results for genes involved in brush border development in small intestinal samples obtained from infant mice (n=9/group) 7 days after challenge with toxigenic ETEC (jf876), nontoxigenic ETEC (jf4763, LT^-/ST^-) PBS controls. Comparisons between data represent ANOVA, Kruskal-Wallis testing where ***p≤0.001, **p≤0.01, and *p≤0.05. **b.** Immunofluorescence images of small intestinal sections showing villin expression (blue), and nuclei (white). **c.** data represent mean villin fluorescence intensity normalized to the intensity of the nuclear signal (DAPI)

(n=4mice/group) **d.** mean villin fluorescence intensity normalized per enterocyte. **e.** representative transmission electron microscopy (TEM) images of the small intestinal brush border from mice challenged with toxin-negative (Δ, left) and toxigenic ETEC (wt, right). **f.** microvillus length ****$p \leq 0.0001$ by Mann Whitney (two-tailed) nonparametric comparisons. Data represent geometric mean length from n=5 mice per group in three independent experiments. g. TEM images from mice challenged with (clockwise from left) jf570 (*eltA*::Km^R), sham PBS controls, or mice challenged with wild type ETEC. h. length of microvilli (dashed horizontal lines represent geometric means). ****$p<0.0001$ by Kruskal-Wallis.

figure 6

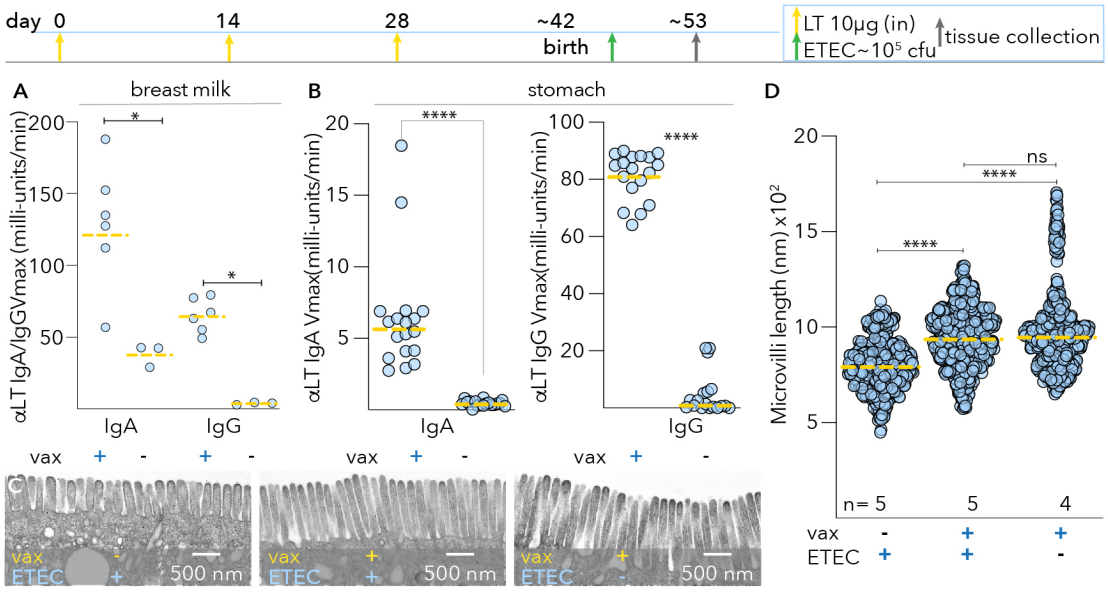

figure 6. Maternal vaccination with LT mitigates microvillus disruption in neonatal mice. Timeline depicts vaccination and challenge (top): maternal intranasal (i.n.) vaccinations with 10 µg LT/immunization (yellow arrows on days 0, 14, 28) and neonatal challenge at 3 days of age (green arrow) followed by sacrifice and tissue collection at 7 days post infection. **A**. Kinetic ELISA data of breast milk anti-LT (IgA, and IgG in immunized dams and un-immunized controls). *<0.05 by Mann-Whitney two-tailed nonparametric testing. **B.** Anti-LT antibodies in the gastric contents of neonatal mice at day 53. **C.** Representative transmission electron microscopy images of brush border microvilli from unvaccinated mice challenged with wild type ETEC (left), vaccinated mice challenged with wild type ETEC, and vaccinated un-challenged controls. **D.** Microvillus lengths (based on image analysis of n=5 mice group) ****<0.0001 Kruskal-Wallis comparisons.

599 **figure 7**

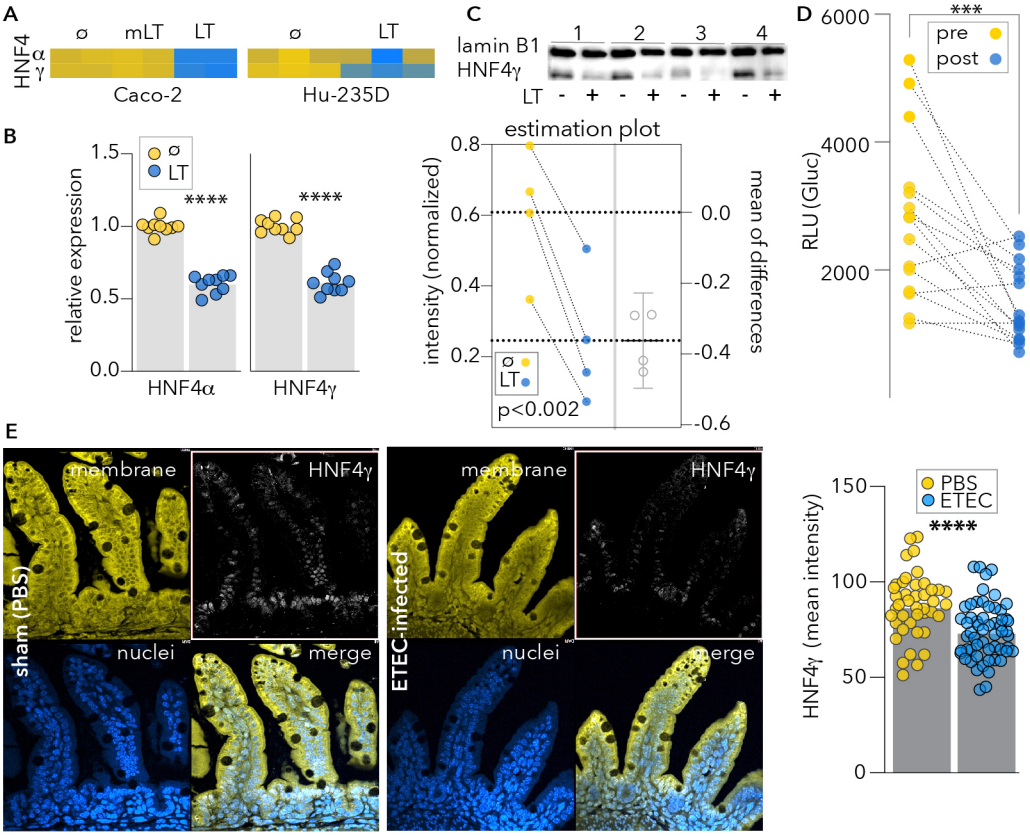

600
601
602 **Enterotoxigenic E. coli heat-labile toxin impairs production of HNF4 nuclear receptors**.
603 **A.** heatmap demonstrating the impact of LT on transcription of paralogous transcription factors
604 HNF4α and HNF4γ in Caco-2cells (left) and ileal enteroids, (Hu-235D, right) ø = untreated, mLT =
605 mutant LT. **B.** qRT-PCR (TaqMan) data confirming decreased transcription of HNF4 transcription
606 factors following treatment of enteroids with LT. **C**. HNF4γ is decreased in nuclear fractions obtained
607 from small intestinal enteroids following treatment with LT. Shown in the HNF4γ immunoblot are
608 samples from 4 independent experiments with graph below representing quantitation of signal
609 intensity normalized to the lamin B1 nuclear protein (p=0.0017, paired t-test, one-tailed). **D.** HNF4
610 transcription *Gaussia* luciferase reporter assay showing decrease in signal following treatment of
611 TR104-transfected Caco-2 cells with LT. 2 experimental replicates (n=15 samples total) *** p<0.001
612 Wilcoxon matched pairs, one-tailed). **E.** Confocal microscopy of representative Ileal sections from
613 sham-challenged (PBS) left, and ETEC-infected mice (right). Immunofluorescence intensity of HNF4γ
614 signal in sections from n=5 control mice, and n=6 ETEC-challenged mice. Membranes (yellow) were
615 strained with CellMask orange (ThermoFisher C10045), nuclei (blue) stained with DAPI, and HNFγ
616 immunostaining represented in white. Each symbol represents a microscopic region of interest. Bars
617 represent geographic means (p<0.0001, Mann-Whitney two-tailed comparisons).
618

supplemental data

supplemental figures

supplemental figure 1

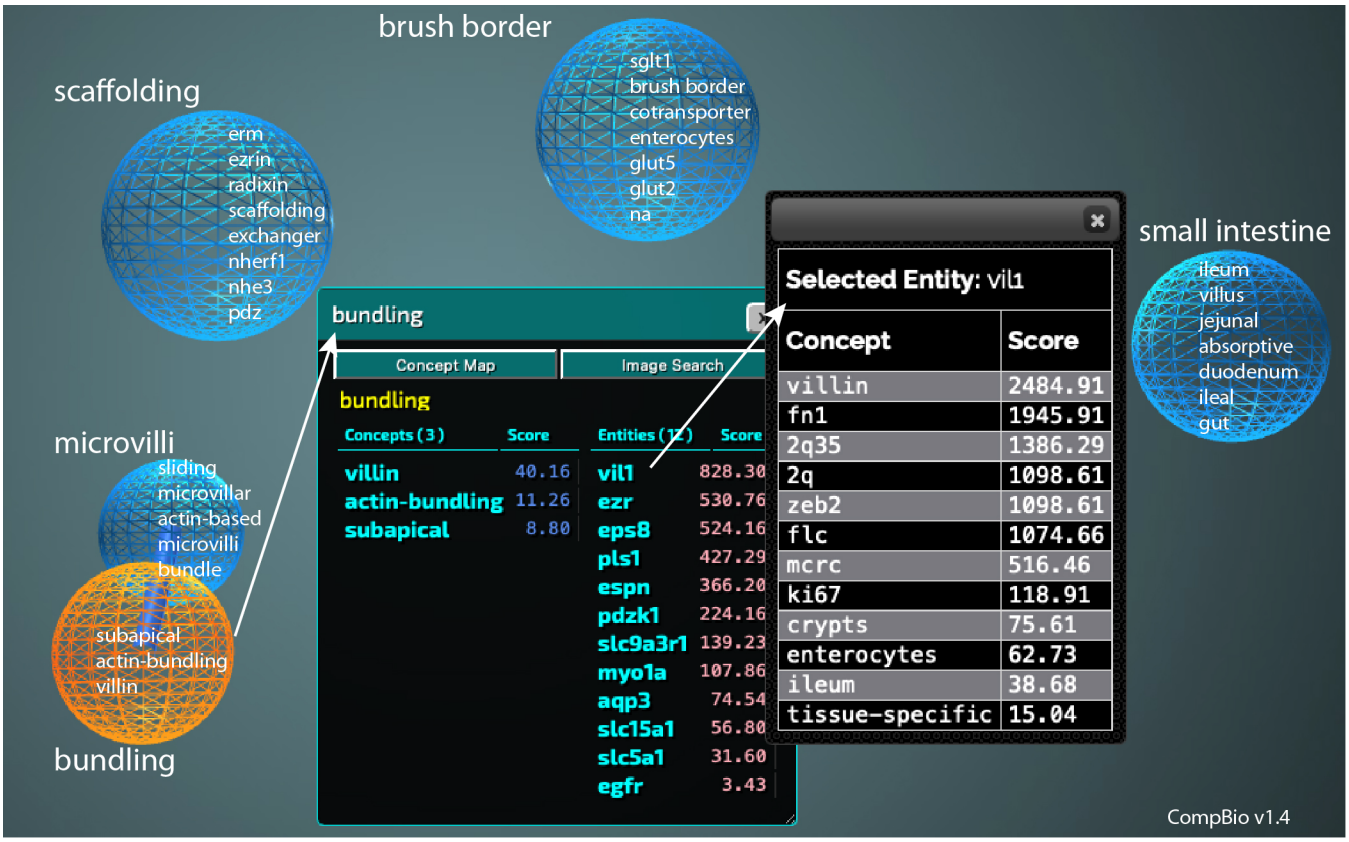

supplemental figure 1. image from representative CombBio (v1.4) analysis of differential gene expression in LT-treated enteroids compared to untreated controls, highlighting themes (spheres) related to biogenesis and function of small intestinal microvilli. Concepts linked within each theme are listed on the corresponding sphere.

supplemental figure 2

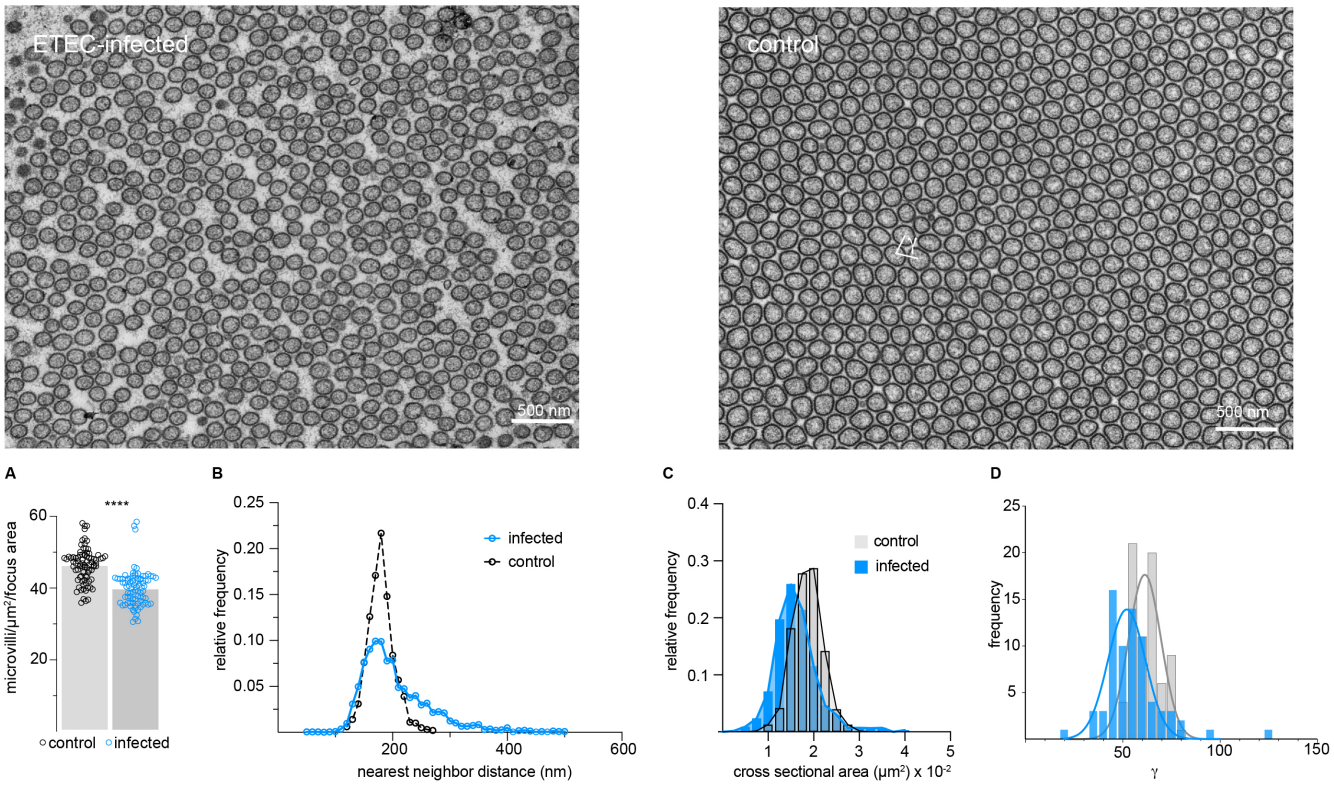

supplemental figure 2. ETEC perturbs the ordered array structure of microvilli. Shown at top are representative TEM cross sections of infected and control mice (n=5) in each group. **A.** density of microvilli/µm^2 (n=83 areas in infected and control). p<0.0001. **B.** distance between centers of adjacent microvilli (n=1001 control, n=2278 infected), p<0.0001 Mann-Whitney. **C.** cross sectional area of microvilli (n=550 control, n=1559 infected) p<0.0001. **D.** g angle distributions of microvilli from control and ETEC-infected mice. (analysis by Mann-Whitney, 2-tailed, nonparametric comparisons).

supplemental figure 3.

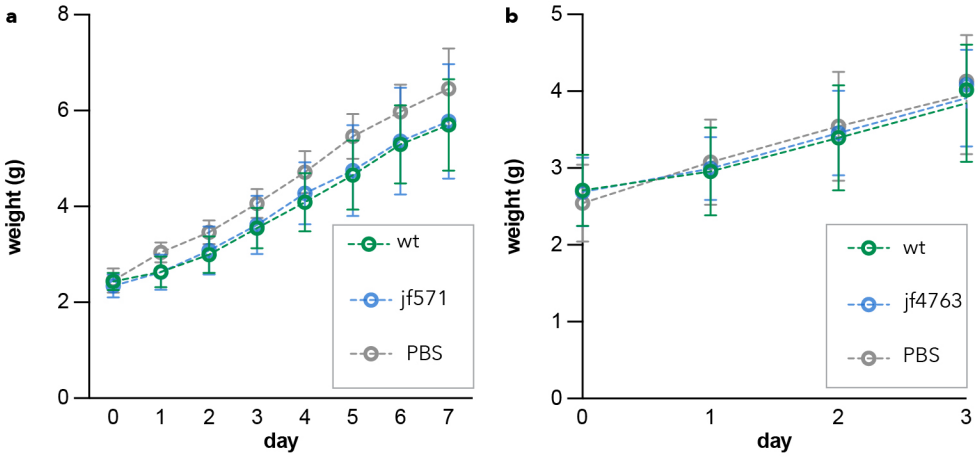

supplemental figure 3. growth kinetics following challenge of suckling mice with ETEC

a. challenge of mice with wild type toxigenic ETEC H10407 (wt), *ΔeltA* mutant (jf571), vs sham challenge (PBS) (n=24/group). data points reflect mean ± sd. **b.** challenge of mice with wild type toxigenic ETEC H10407 (wt) (n=21); *ΔeltA, ΔestH, ΔestP* nontoxigenic mutant (jf4763), vs sham challenge (PBS) (n=20/group).

supplemental figure 4

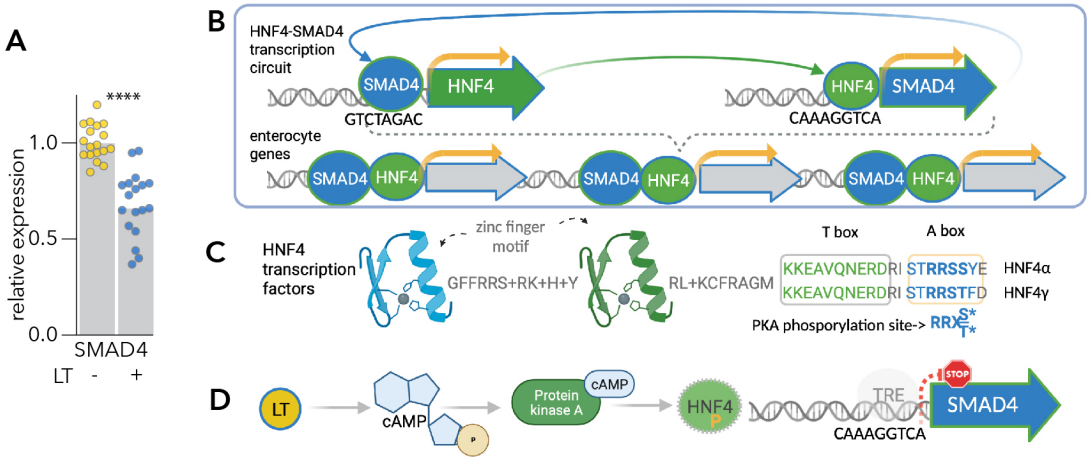

Supplemental figure 4. LT interrupts HNF4-SMAD4 mediated transcription. **A.** treatment of human-derived small intestinal enteroids (Hu235D) with LT leads to decreased SMAD4 transcription. Shown are TaqMan probe results from two independent experiments of polarized epithelial monolayers treated with LT. n=3 biological replicates x 3 technical replicates/ experiment =18 data points. ****p<0.0001 by Mann Whitney, two-tailed nonparametric comparisons to untreated cells. **B.** depiction of the HNF4-SMAD4 reciprocal transcription factor activation in which HNF4 activates transcription of SMAD4 and *vice versa* as (Chen, *et* al[71]). **C.** PKA-mediated phosphorylation of HNF4 paralogs interrupts a DNA-binding module (Viollet, *et al*[70].). **D.** Summary of proposed mechanism by which LT leads to depletion of transcription factors essential for enterocyte differentiation. LT-mediated activation of PKA leads to phosphorylation of HNF4 rendering these transcription factors incapable of binding to *cis* transcriptional response elements (TRE) in promotors of target genes including SMAD4. Decreased SMAD4 transcription in turn depletes available HNF4.

665
666 **supplemental tables**
667 supplemental table 1

strains and plasmids used in these studies		
bacterial strains		
strain designation	description	source
H10407	wild type ETEC strain, *eltAB*, *estP*, *estH*	[91]
jf571	*eltA*::Km^R derivative of H10407	[92]
jf876	*lacZYA*::Km^R derivative of H10407	[92]
jf4763	*eltAB*::Sp^R, estP::Km^R, estH::Cm^R toxin-negative derivative of H10407.	this study
plasmids		
designation	description	source
TR104	6 copies of HNF4 transcriptional response element upstream of Gaussia luciferase reporter (Gaussia-Dura Luc). Km^R, Pm^R	GeneCopoeia
SEAP-PA01	secreted alkaline phosphatase; CMV promotor; Amp^R	GeneCopoeia
Sp^R spectinomycin resistant; Km^R kanamycin resistant; Cm^R chloramphenicol resistant; Pm^R puromycin resistant, Amp^R ampicillin resistant		

668
669

670
671 supplemental table 2 primers and probes for gene expression

RT-PCR primers			
gene	species	primer sequence (5'-3')	
		forward	reverse
SLC19A3	Human	TTCCTGGATTTACCCCACTG	TATGTCCAAACGGGGAAGA
VIL1	Human	CTGAGCGCCCAAGTCAAAG	AGCAGTCACCATCGAAGAAGC
MYO1A	Human	ACAGGCGAGAGTGGATCAG	GCACTGGGTTAGACTGTAGCAG
MYO7B	Human	TGGACGCCTCAGACGTGAT	CTGGTGACAAATTCCCCTCGG
SP-1	Human	CCATACCCCTTAACCCCG	GAATTTTCACTAATGTTTCCCACC
GAPDH	Human	CATTTCCTGGTATGACAACGA	CTTCCTCTTGTGCTCTTGCT
b-actin	Human	CATCCTGCGTCTGGACCT	TAATGTCACGCACGATTTCC
Ezr	Mouse	CAATCAACGTCCGGGTGAC	GCCAATCGTCTTTACCACCTGA
Vil1	Mouse	TCAAAGGCTCTCTCAACATCAC	AGCAGTCACCATCGAAGAAGC
Espn	Mouse	GGAAATACAGAGGGCGAAAGA	AGAAGCCGAGAGACTCCTATTA
Cdhr2	Mouse	GGCCTCGATTCTACAGCCAAT	GCTCAGAGCCATTCTCAGTCAC
Myo7B	Mouse	AGGGGACCTGAATGAGGCT	GCGGCTGTAGTAGATTTGTACCT
Ebp50	Mouse	AGGGTCCAAATGGCTACGG	CTCCACCAATCGGTCTCCAG
GAPDH	Mouse	AGGTCGGTGTGAACGGATTTG	TGTAGACCATGTAGTTGAGGTCA
TaqMan probes			
gene	species	chromosome	location
HNF4α	Human	20	44355801 - 44432845
HNF4γ	Human	8	75407567 - 75566834
SMAD4	Human	18	51030213 - 51085042

672

673

674

675 supplemental table 3

differential gene expression in gastrointestinal cells following treatment with LT			
response to LT	dataset	genes (n) $p<0.05$*	genes (n) $p<10^{-5}$*
higher	Caco-2	5,631	3,832
	ileal enteroids	2138	746
	both†	877	268
lower	Caco-2	5,263	3,687
	ileal enteroids	1,839	561
	both†	1,013	311

*differentially expressed genes identified by DESeq2[90]
† overlap in up- and downregulated genes was statistically higher than expected by random selection ($p<10^{-10}$, binomial distribution testing)

676
677

678 supplemental table 4.

supplemental table 4. Transcription factor target sequence enrichment among genes differentially regulated in both RNA-seq datasets

transcription factor	target designation	target motif	Total pathway size	Number of significant genes	FDR-adjusted P value
		transcription factor target			
	*877 genes upregulated by LT in both RNA-seq datasets**				
AP1 / JUN	TGANTCA_V$AP1_C	TGANTCA	1108	91	4.2E-03
LEF1	CTTTGT_V$LEF1_Q2	CTTTGT	1939	142	4.2E-03
USF	V$USF_C	NCACGTGN	278	32	5.2E-03
	*1,013 genes downregulated by LT in both RNA-seq datasets**				
HNF4αγ	V$HNF4_01	NNNRGGNCAAAGKTCANNN	269	37	1.9E-04
HNF4αγ	V$HNF4_01_B	NRGGNCAAAGGTCAN	249	32	2.6E-03
USF	V$USF_02	NNRNCACGTGNYNN	270	32	8.8E-03
SREBP1	TCANNTGAY_V$SREBP1_01	TCANNTGAY	469	47	9.9E-03
NR2F2/COUP	V$COUP_01	TGAMCTTTGMMCYT	260	30	0.015
IRF1	STTTCRNTTT_V$IRF_Q6	STTTCRNTTT	185	23	0.025
USF	V$USF_01	NNRYCACGTGRYNN	254	28	0.038
HNF1	RGTTAMWNATT_V$HNF1_01	RGTTAMWNATT	72	12	0.044

679 *differentially expressed genes identified by DESeq2[90] $p<0.05$
680

681

682 supplemental table 5.

antibodies used in these studies		
Specificity	description	source/reference
villin	Villin antibody (BDID2C3), mouse monoclonal IgG1	Santa Cruz sc-66022
mouse IgG	Goat anti-Mouse (H&L) IgG, highly cross-adsorbed antibody conjugated to Alexa Fluor 488	ThermoFisher A-11029
mouse IgA	Pre-absorbed, affinity purified goat anti-mouse IgA conjugated to HRP	Santa Cruz sc-3793
mouse IgG	Affinity purified horse anti-mouse IgG conjugated to HRP	Cell Signaling 7076
HNF4γ	rabbit polyclonal IgG against residues 327-408 of human HNF4γ	ThermoFisher 25801-1-AP
HNF4α	monoclonal IgG2a clone K9218) vs Baculovirus-expressed recombinant human HNF4α (aa 3-49)	ThermoFisher MA1-199

683

supplemental table 6

links to original images	
item	DOI
figure 4b	10.6084/m9.figshare.19251848
figure 4c	10.6084/m9.figshare.19251845
figure 5b	10.6084/m9.figshare.19287353
figure 5e	10.6084/m9.figshare.19251911
figure 5g	10.6084/m9.figshare.19251926
figure 6c	10.6084/m9.figshare.19251938
Figure 7c	10.6084/m9.figshare.19742413

references

1 Collaborators, G. B. D. D. D. Quantifying risks and interventions that have affected the burden of diarrhoea among children younger than 5 years: an analysis of the Global Burden of Disease Study 2017. *Lancet Infect Dis* **20**, 37-59, doi:10.1016/S1473-3099(19)30401-3 (2020).

2 Sack, R. B. *et al.* Enterotoxigenic Escherichia coli isolated from patients with severe cholera-like disease. *J Infect Dis* **123**, 378-385 (1971).

3 Kotloff, K. L. *et al.* Burden and aetiology of diarrhoeal disease in infants and young children in developing countries (the Global Enteric Multicenter Study, GEMS): a prospective, case-control study. *Lancet* **382**, 209-222, doi:10.1016/S0140-6736(13)60844-2 (2013).

4 Kotloff, K. L. *et al.* The incidence, aetiology, and adverse clinical consequences of less severe diarrhoeal episodes among infants and children residing in low-income and middle-income countries: a 12-month case-control study as a follow-on to the Global Enteric Multicenter Study (GEMS). *Lancet Glob Health* **7**, e568-e584, doi:10.1016/S2214-109X(19)30076-2 (2019).

5 Steffen, R., Hill, D. R. & DuPont, H. L. Traveler's diarrhea: a clinical review. *JAMA* **313**, 71-80, doi:10.1001/jama.2014.17006 (2015).

6 Khalil, I. A. *et al.* Morbidity and mortality due to shigella and enterotoxigenic Escherichia coli diarrhoea: the Global Burden of Disease Study 1990-2016. *Lancet Infect Dis* **18**, 1229-1240, doi:10.1016/S1473-3099(18)30475-4 (2018).

7 Nasrin, D. *et al.* Pathogens associated with linear growth faltering in children with diarrhea and impact of antibiotic treatment: The Global Enteric Multicenter Study. *J Infect Dis*, doi:10.1093/infdis/jiab434 (2021).

8 Qadri, F. *et al.* Disease burden due to enterotoxigenic Escherichia coli in the first 2 years of life in an urban community in Bangladesh. *Infect Immun* **75**, 3961-3968, doi:10.1128/IAI.00459-07 (2007).

9 Black, R. E., Brown, K. H. & Becker, S. Effects of diarrhea associated with specific enteropathogens on the growth of children in rural Bangladesh. *Pediatrics* **73**, 799-805 (1984).

10 Anderson, J. D. t. *et al.* Burden of enterotoxigenic Escherichia coli and shigella non-fatal diarrhoeal infections in 79 low-income and lower middle-income countries: a modelling analysis. *Lancet Glob Health* **7**, e321-e330, doi:10.1016/S2214-109X(18)30483-2 (2019).

11 Caulfield, L. E., de Onis, M., Blossner, M. & Black, R. E. Undernutrition as an underlying cause of child deaths associated with diarrhea, pneumonia, malaria, and measles. *Am J Clin Nutr* **80**, 193-198, doi:10.1093/ajcn/80.1.193 (2004).

12 Checkley, W. *et al.* Multi-country analysis of the effects of diarrhoea on childhood stunting. *Int J Epidemiol* **37**, 816-830, doi:10.1093/ije/dyn099 (2008).

13 Klipstein, F. A., Short, H. B., Engert, R. F., Jean, L. & Weaver, G. A. Contamination of the small intestine by enterotoxigenic coliform bacteria among the rural population of Haiti. *Gastroenterology* **70**, 1035-1041 (1976).

14 Klipstein, F. A., Holdeman, L. V., Corcino, J. J. & Moore, W. E. Enterotoxigenic intestinal bacteria in tropical sprue. *Ann Intern Med* **79**, 632-641 (1973).

15 Klipstein, F. A., Engert, R. F. & Short, H. B. Enterotoxigenicity of colonising coliform bacteria in tropical sprue and blind-loop syndrome. *Lancet* **2**, 342-344 (1978).

16 Brunser, O., Eidelman, S. & Klipstein, F. A. Intestinal morphology of rural Haitians. A comparison between overt tropical sprue and asymptomatic subjects. *Gastroenterology* **58**, 655-668 (1970).

17 Mathan, M., Mathan, V. I. & Baker, S. J. An electron-microscopic study of jejunal mucosal morphology in control subjects and in patients with tropical sprue in southern India. *Gastroenterology* **68**, 17-32 (1975).

18 Fleckenstein, J. M. *et al.* Molecular mechanisms of enterotoxigenic Escherichia coli infection. *Microbes Infect* **12**, 89-98, doi:S1286-4579(09)00235-4 [pii]
10.1016/j.micinf.2009.10.002 (2010).

19 Tsai, S. C., Noda, M., Adamik, R., Moss, J. & Vaughan, M. Enhancement of choleragen ADP-ribosyltransferase activities by guanyl nucleotides and a 19-kDa membrane protein. *Proc Natl Acad Sci U S A* **84**, 5139-5142. (1987).

20 Lodish H, B. A., Zipursky SL, Matsudaira P, Baltimore D, Darnell J. in *Molecular Cell Biology* (W. H. Freeman, 2000).

21 Sassone-Corsi, P. Transcription factors responsive to cAMP. *Annu Rev Cell Dev Biol* **11**, 355-377, doi:10.1146/annurev.cb.11.110195.002035 (1995).

22 Sassone-Corsi, P. The cyclic AMP pathway. *Cold Spring Harb Perspect Biol* **4**, doi:10.1101/cshperspect.a011148 (2012).

23 Zambon, A. C. *et al.* Gene expression patterns define key transcriptional events in cell-cycle regulation by cAMP and protein kinase A. *Proc Natl Acad Sci U S A* **102**, 8561-8566, doi:10.1073/pnas.0503363102 (2005).

24 Hansson, H. A., Lange, S., Lonnroth, I., Rozell, B. & Tinberg, H. Cytoskeletal disarrangement in rat intestinal epithelium after in vivo exposure to secretagogues. *Acta Pathol Microbiol Immunol Scand [B]* **92**, 93-99 (1984).

25 Mathan, M. M., Chandy, G. & Mathan, V. I. Ultrastructural changes in the upper small intestinal mucosa in patients with cholera. *Gastroenterology* **109**, 422-430, doi:10.1016/0016-5085(95)90329-1 (1995).

26 Asakura, H., Tsuchiya, M., Watanabe, Y., Enomoto, Y. & Morita, A. Electron microscopic study on the jejunal mucosa in human cholera. *Gut* **15**, 531-544, doi:10.1136/gut.15.7.531 (1974).

27 Platts-Mills, J. A. *et al.* Association between enteropathogens and malnutrition in children aged 6-23 mo in Bangladesh: a case-control study. *Am J Clin Nutr* **105**, 1132-1138, doi:10.3945/ajcn.116.138800 (2017).

28 Ilantzis, C., DeMarte, L., Screaton, R. A. & Stanners, C. P. Deregulated expression of the human tumor marker CEA and CEA family member CEACAM6 disrupts tissue architecture and blocks colonocyte differentiation. *Neoplasia* **4**, 151-163, doi:10.1038/sj.neo.7900201 (2002).

29 Tadjali, M., Seidelin, J. B., Olsen, J. & Troelsen, J. T. Transcriptome changes during intestinal cell differentiation. *Biochim Biophys Acta* **1589**, 160-167, doi:10.1016/s0167-4889(02)00170-2 (2002).

30 Crawley, S. W., Mooseker, M. S. & Tyska, M. J. Shaping the intestinal brush border. *J Cell Biol* **207**, 441-451, doi:10.1083/jcb.201407015 (2014).

31 Postema, M. M., Grega-Larson, N. E., Neininger, A. C. & Tyska, M. J. IRTKS (BAIAP2L1) Elongates Epithelial Microvilli Using EPS8-Dependent and Independent Mechanisms. *Curr Biol* **28**, 2876-2888 e2874, doi:10.1016/j.cub.2018.07.022 (2018).

32 Tyska, M. J. *et al.* Myosin-1a is critical for normal brush border structure and composition. *Mol Biol Cell* **16**, 2443-2457, doi:10.1091/mbc.e04-12-1116 (2005).

33 Crawley, S. W., Weck, M. L., Grega-Larson, N. E., Shifrin, D. A., Jr. & Tyska, M. J. ANKS4B Is Essential for Intermicrovillar Adhesion Complex Formation. *Dev Cell* **36**, 190-200, doi:10.1016/j.devcel.2015.12.022 (2016).

34 He, L., Vasiliou, K. & Nebert, D. W. Analysis and update of the human solute carrier (SLC) gene superfamily. *Hum Genomics* **3**, 195-206, doi:10.1186/1479-7364-3-2-195 (2009).

35 Manary, M. J. *et al.* Perturbed zinc homeostasis in rural 3-5-y-old Malawian children is associated with abnormalities in intestinal permeability attributed to tropical enteropathy. *Pediatr Res* **67**, 671-675, doi:10.1203/PDR.0b013e3181da44dc (2010).

36 Reidling, J. C., Lambrecht, N., Kassir, M. & Said, H. M. Impaired intestinal vitamin B1 (thiamin) uptake in thiamin transporter-2-deficient mice. *Gastroenterology* **138**, 1802-1809, doi:10.1053/j.gastro.2009.10.042 (2010).

37 Subramanian, V. S., Marchant, J. S. & Said, H. M. Targeting and trafficking of the human thiamine transporter-2 in epithelial cells. *J Biol Chem* **281**, 5233-5245, doi:10.1074/jbc.M512765200 (2006).

38 Said, H. M., Balamurugan, K., Subramanian, V. S. & Marchant, J. S. Expression and functional contribution of hTHTR-2 in thiamin absorption in human intestine. *American journal of physiology. Gastrointestinal and liver physiology* **286**, G491-498, doi:10.1152/ajpgi.00361.2003 (2004).

39 Nabokina, S. M., Subramanian, V. S., Valle, J. E. & Said, H. M. Adaptive regulation of human intestinal thiamine uptake by extracellular substrate level: a role for THTR-2 transcriptional regulation. *American journal of physiology. Gastrointestinal and liver physiology* **305**, G593-599, doi:10.1152/ajpgi.00237.2013 (2013).

40 Nabokina, S. M. & Said, H. M. Characterization of the 5'-regulatory region of the human thiamin transporter SLC19A3: in vitro and in vivo studies. *Am J Physiol Gastrointest Liver Physiol* **287**, G822-829, doi:10.1152/ajpgi.00234.2004 (2004).

41 Nabokina, S. M., Reidling, J. C. & Said, H. M. Differentiation-dependent up-regulation of intestinal thiamin uptake: cellular and molecular mechanisms. *J Biol Chem* **280**, 32676-32682, doi:10.1074/jbc.M505243200 (2005).

42 Blanton, L. V., Barratt, M. J., Charbonneau, M. R., Ahmed, T. & Gordon, J. I. Childhood undernutrition, the gut microbiota, and microbiota-directed therapeutics. *Science* **352**, 1533, doi:10.1126/science.aad9359 (2016).

43 Wang, J., Vasaikar, S., Shi, Z., Greer, M. & Zhang, B. WebGestalt 2017: a more comprehensive, powerful, flexible and interactive gene set enrichment analysis toolkit. *Nucleic Acids Res.* **45**, W130-W137, doi:10.1093/nar/gkx356 (2017).

44 Liberzon, A. *et al.* The Molecular Signatures Database (MSigDB) hallmark gene set collection. *Cell Syst* **1**, 417-425, doi:10.1016/j.cels.2015.12.004 (2015).

45 Nakamura, T., Datta, R., Sherman, M. L. & Kufe, D. Regulation of c-jun gene expression by cAMP in HL-60 myeloid leukemia cells. *J Biol Chem* **265**, 22011-22015 (1990).

46 Wang, P. Y. *et al.* c-Jun enhances intestinal epithelial restitution after wounding by increasing phospholipase C-gamma1 transcription. *Am J Physiol Cell Physiol* **312**, C367-C375, doi:10.1152/ajpcell.00330.2016 (2017).

47 San Roman, A. K., Aronson, B. E., Krasinski, S. D., Shivdasani, R. A. & Verzi, M. P. Transcription factors GATA4 and HNF4A control distinct aspects of intestinal homeostasis in conjunction with transcription factor CDX2. *J Biol Chem* **290**, 1850-1860, doi:10.1074/jbc.M114.620211 (2015).

48 Chen, L. *et al.* The nuclear receptor HNF4 drives a brush border gene program conserved across murine intestine, kidney, and embryonic yolk sac. *Nature communications* **12**, 2886, doi:10.1038/s41467-021-22761-5 (2021).

49 Dankel, S. N., Hoang, T., Flageng, M. H., Sagen, J. V. & Mellgren, G. cAMP-mediated regulation of HNF-4alpha depends on the level of coactivator PGC-1alpha. *Biochim Biophys Acta* **1803**, 1013-1019, doi:10.1016/j.bbamcr.2010.05.008 (2010).

50 Khalil, I. *et al.* Enterotoxigenic Escherichia coli (ETEC) vaccines: Priority activities to enable product development, licensure, and global access. *Vaccine* **39**, 4266-4277, doi:10.1016/j.vaccine.2021.04.018 (2021).

51 Sheikh, A. *et al.* CEACAMs serve as toxin-stimulated receptors for enterotoxigenic Escherichia coli. *Proc Natl Acad Sci U S A* **117**, 29055-29062, doi:10.1073/pnas.2012480117 (2020).

52 Sheikh, A. *et al.* Enterotoxigenic Escherichia coli degrades the host MUC2 mucin barrier to facilitate critical pathogen-enterocyte interactions in human small intestine. *Infect Immun*, IAI0057221, doi:10.1128/IAI.00572-21 (2021).

53 Harris, J. B. Cholera: Immunity and Prospects in Vaccine Development. *J Infect Dis* **218**, S141-S146, doi:10.1093/infdis/jiy414 (2018).

54 Pipaliya, N. *et al.* Spectrum of chronic small bowel diarrhea with malabsorption in Indian subcontinent: is the trend really changing? *Intest Res* **14**, 75-82, doi:10.5217/ir.2016.14.1.75 (2016).

55 Ghoshal, U. C., Srivastava, D., Verma, A. & Ghoshal, U. Tropical sprue in 2014: the new face of an old disease. *Curr Gastroenterol Rep* **16**, 391, doi:10.1007/s11894-014-0391-3 (2014).

56 Dutta, A. K., Balekuduru, A. & Chacko, A. Spectrum of malabsorption in India--tropical sprue is still the leader. *J Assoc Physicians India* **59**, 420-422 (2011).

57 Klipstein, F. A. & Falaiye, J. M. Tropical sprue in expatriates from the tropics living in the continental United States. *Medicine (Baltimore)* **48**, 475-491 (1969).

58 Klipstein, F. A. Tropical sprue in travelers and expatriates living abroad. *Gastroenterology* **80**, 590-600 (1981).

59 Kelly, P. *et al.* Gene expression profiles compared in environmental and malnutrition enteropathy in Zambian children and adults. *EBioMedicine* **70**, 103509, doi:10.1016/j.ebiom.2021.103509 (2021).

60 Zyambo, K. *et al.* Reduced Fractional Absorption of Zinc in Children With Environmental Enteropathy in Zambia. *J Pediatr Gastroenterol Nutr* **74**, 277-283, doi:10.1097/MPG.0000000000003292 (2022).

61 Long, J. M. *et al.* Zinc Absorption from Micronutrient Powders Is Low in Bangladeshi Toddlers at Risk of Environmental Enteric Dysfunction and May Increase Dietary Zinc Requirements. *J Nutr* **149**, 98-105, doi:10.1093/jn/nxy245 (2019).

62 Lindenmayer, G. W., Stoltzfus, R. J. & Prendergast, A. J. Interactions between zinc deficiency and environmental enteropathy in developing countries. *Adv Nutr* **5**, 1-6, doi:10.3945/an.113.004838 (2014).

63 Roy, S. K. *et al.* Impact of zinc supplementation on intestinal permeability in Bangladeshi children with acute diarrhoea and persistent diarrhoea syndrome. *J Pediatr Gastroenterol Nutr* **15**, 289-296, doi:10.1097/00005176-199210000-00010 (1992).

64 Dhingra, U. *et al.* Lower-Dose Zinc for Childhood Diarrhea - A Randomized, Multicenter Trial. *N Engl J Med* **383**, 1231-1241, doi:10.1056/NEJMoa1915905 (2020).

65 Kuhlmann, F. M. *et al.* Conservation and global distribution of non-canonical antigens in Enterotoxigenic Escherichia coli. *PLoS Negl Trop Dis* **13**, e0007825, doi:10.1371/journal.pntd.0007825 (2019).

66 Zhang, X. *et al.* Genome-wide analysis of cAMP-response element binding protein occupancy, phosphorylation, and target gene activation in human tissues. *Proc Natl Acad Sci U S A* **102**, 4459-4464, doi:10.1073/pnas.0501076102 (2005).

67 Mayr, B. & Montminy, M. Transcriptional regulation by the phosphorylation-dependent factor CREB. *Nat Rev Mol Cell Biol* **2**, 599-609 (2001).

68 Delghandi, M. P., Johannessen, M. & Moens, U. The cAMP signalling pathway activates CREB through PKA, p38 and MSK1 in NIH 3T3 cells. *Cell Signal* **17**, 1343-1351, doi:10.1016/j.cellsig.2005.02.003 (2005).

69 Rohlff, C., Ahmad, S., Borellini, F., Lei, J. & Glazer, R. I. Modulation of transcription factor Sp1 by cAMP-dependent protein kinase. *J Biol Chem* **272**, 21137-21141, doi:10.1074/jbc.272.34.21137 (1997).

70 Viollet, B., Kahn, A. & Raymondjean, M. Protein kinase A-dependent phosphorylation modulates DNA-binding activity of hepatocyte nuclear factor 4. *Molecular and cellular biology* **17**, 4208-4219, doi:10.1128/MCB.17.8.4208 (1997).

71 Chen, L. *et al.* A reinforcing HNF4-SMAD4 feed-forward module stabilizes enterocyte identity. *Nat Genet* **51**, 777-785, doi:10.1038/s41588-019-0384-0 (2019).

72 de Rooij, J. *et al.* Epac is a Rap1 guanine-nucleotide-exchange factor directly activated by cyclic AMP. *Nature* **396**, 474-477, doi:10.1038/24884 (1998).

73 Bos, J. L., de Rooij, J. & Reedquist, K. A. Rap1 signalling: adhering to new models. *Nat Rev Mol Cell Biol* **2**, 369-377, doi:10.1038/35073073 (2001).

74 Frische, E. W. & Zwartkruis, F. J. Rap1, a mercenary among the Ras-like GTPases. *Dev Biol* **340**, 1-9, doi:10.1016/j.ydbio.2009.12.043 (2010).

75 Ogryzko, V. V., Schiltz, R. L., Russanova, V., Howard, B. H. & Nakatani, Y. The transcriptional coactivators p300 and CBP are histone acetyltransferases. *Cell* **87**, 953-959, doi:10.1016/s0092-8674(00)82001-2 (1996).

76 Pattabiraman, D. R. *et al.* Activation of PKA leads to mesenchymal-to-epithelial transition and loss of tumor-initiating ability. *Science* **351**, aad3680, doi:10.1126/science.aad3680 (2016).

77 Anders, S. & Huber, W. Differential expression analysis for sequence count data. *Genome Biol* **11**, R106, doi:10.1186/gb-2010-11-10-r106 (2010).

78 Benjamini, Y. & Hochberg, Y. Controlling the False Discovery Rate: A Practical and Powerful Approach to Multiple Testing. *Journal of the Royal Statistical Society. Series B (Methodological)* **57**, 289-300, doi:10.2307/2346101 (1995).

79 Kanehisa, M., Furumichi, M., Sato, Y., Ishiguro-Watanabe, M. & Tanabe, M. KEGG: integrating viruses and cellular organisms. *Nucleic Acids Res* **49**, D545-D551, doi:10.1093/nar/gkaa970 (2021).

80 Gene Ontology, C. The Gene Ontology resource: enriching a GOld mine. *Nucleic Acids Res* **49**, D325-D334, doi:10.1093/nar/gkaa1113 (2021).

81 Delannoy-Bruno, O. *et al.* Evaluating microbiome-directed fibre snacks in gnotobiotic mice and humans. *Nature* **595**, 91-95, doi:10.1038/s41586-021-03671-4 (2021).

82 Sabui, S. *et al.* Hypoxia inhibits colonic uptake of the microbiota-generated forms of vitamin B1 via HIF-1alpha-mediated transcriptional regulation of their transporters. *J Biol Chem* **298**, 101562, doi:10.1016/j.jbc.2022.101562 (2022).

83 Howe, K. L. *et al.* Ensembl 2021. *Nucleic Acids Res* **49**, D884-D891, doi:10.1093/nar/gkaa942 (2021).

84 Matys, V. *et al.* TRANSFAC and its module TRANSCompel: transcriptional gene regulation in eukaryotes. *Nucleic Acids Res* **34**, D108-110, doi:10.1093/nar/gkj143 (2006).
85 Wang, J., Vasaikar, S., Shi, Z., Greer, M. & Zhang, B. WebGestalt 2017: a more comprehensive, powerful, flexible and interactive gene set enrichment analysis toolkit. *Nucleic Acids Res* **45**, W130-W137, doi:10.1093/nar/gkx356 (2017).
86 Sack, D. A., Huda, S., Neogi, P. K., Daniel, R. R. & Spira, W. M. Microtiter ganglioside enzyme-linked immunosorbent assay for vibrio and Escherichia coli heat-labile enterotoxins and antitoxin. *J Clin Microbiol* **11**, 35-40 (1980).
87 Tsang, V. C., Wilson, B. C. & Maddison, S. E. Kinetic studies of a quantitative single-tube enzyme-linked immunosorbent assay. *Clinical chemistry* **26**, 1255-1260 (1980).
88 Roy, K., Hamilton, D. J., Munson, G. P. & Fleckenstein, J. M. Outer Membrane Vesicles Induce Immune Responses to Virulence Proteins and Protect against Colonization by Enterotoxigenic Escherichia coli. *Clin Vaccine Immunol* **18**, 1803-1808, doi:10.1128/CVI.05217-11 (2011).
89 Sixma, T. K. *et al.* Refined structure of Escherichia coli heat-labile enterotoxin, a close relative of cholera toxin. *J Mol Biol* **230**, 890-918, doi:10.1006/jmbi.1993.1209 (1993).
90 Love, M. I., Huber, W. & Anders, S. Moderated estimation of fold change and dispersion for RNA-seq data with DESeq2. *Genome Biol* **15**, 550, doi:10.1186/s13059-014-0550-8 (2014).
91 Evans, D. J., Jr. & Evans, D. G. Three characteristics associated with enterotoxigenic Escherichia coli isolated from man. *Infect Immun* **8**, 322-328 (1973).
92 Dorsey, F. C., Fischer, J. F. & Fleckenstein, J. M. Directed delivery of heat-labile enterotoxin by enterotoxigenic Escherichia coli. *Cell Microbiol* **8**, 1516-1527, doi:10.1111/j.1462-5822.2006.00736.x (2006).

acknowledgements

JMF was supported by funding from the National Institute of Allergy and Infectious Diseases (NIAID) of the National Institutes of Health (NIH) R01 AI126887, R01 AI089894, U01 AI095473; and the Department of Veterans Affairs (5I01BX001469-05). Research conducted by AS was also supported by National Institute of Allergy and Infectious Diseases of the National Institutes of Health under Award Number T32AI007172. We thank the Genome Technology Access Center in the Department of Genetics at Washington University School of Medicine for help with genomic analysis. The Center is partially supported by NCI Cancer Center Support Grant #P30 CA91842 to the Siteman Cancer Center and by ICTS/CTSA Grant# UL1TR002345 from the National Center for Research Resources (NCRR), a component of the National Institutes of Health (NIH), and NIH Roadmap for Medical Research. HS was supported by funding from the Department of Veterans Affairs (I01BX001142) and the National Institutes of Health (DK5606 and AA018071). The content is solely the responsibility of the authors and does not necessarily represent the official views of the National Institutes of Health, or the Department of Veterans Affairs.

interests declaration

R.D.H. and C.S. may receive royalty income based on the CompBio technology developed by R.D.H. and licensed by Washington University to PercayAI.